660

Aerosol-Cloud-Radiation Interactions and their Impact on ECMWF/MACC Forecasts

J.-J. Morcrette[1], A. Benedetti[1], A. Ghelli[1], J.W. Kaiser[1], A.M. Tompkins[2]

[1]European Centre for Medium-Range Weather Forecasts, Reading, UK
[2]Earth System Physics, ICTP, Trieste, Italy

Research Department

December 2011

Abstract

Prognostic aerosols were experimentally introduced in the ECMWF Integrated Forecasting System (IFS) as part of the GEMS project in 2005. Their representation was refined as part of the MACC project, starting in 2009. Here, the MACC aerosol system is used to explore the impact of different levels of interactions between the aerosols and either the radiation and/or the cloud processes on radiation and precipitation fields, and objective scores. Ten-day forecasts including fully interactive aerosols are compared to forecasts with aerosols specified from the analysis and kept constant thereafter. Whereas the temporal variability of the prognostic aerosols is shown to have strong local effects on surface parameters, the impact on objective scores is much smaller.

1 Introduction

In the 1990s, a number of climate-oriented groups developed global models including a prognostic aerosol with a focus on one or another aerosol type (e.g., dust for Joussaume, 1990; Tegen and Fung, 1994; carbonaceous aerosols for Liousse et al., 1996; sea salt for Genthon, 1992; Gong et al., 1997; sulfate for Chin et al., 1996). In parallel to these efforts, models were also tested for their conservation properties (Guelle et al., 1998a, 1998b; Dentener et al., 1999). Looking at another methodological aspect, experiments were also run aiming at defining the best configuration to ensure reasonable aerosol forecasts (Jeuken et al., 1996; Feichter and Lohmann, 1999). By the mid-1990's, the aerosol modelling community felt that a climate GCM run at relatively low resolution from "cold-start" or climatological initial conditions would likely be diverging in terms of its main prognostic variables (temperature, pressure, wind, humidity) and thus would make the associated aerosol variables unrealistic. Most aerosol simulations (apart from climate simulations following climate scenarios such as those run for the Intergovernmental Panel on Climate Change model intercomparison) use atmospheric forcings (in terms of pressure, temperature, humidity, wind, ...) derived from meteorological analyses or re-analyses (see AEROCOM (AEROsol Comparisons between Observations and Models) web site). This has the advantage that the meteorology follows the real day-to-day synoptic variability and verification can focus on the aerosol model.

The first multi-aerosol model simulations, run with a forcing of the basic meteorology from an operational analysis every six, 12 or 24 hours, started to appear at the end of the 1990s (Tegen et al., 1997) and have been the common set-up ever since (Guelle et al., 2000; Clarke et al., 2001; Chin et al., 2002; Grini et al., 2002; Penner et al., 2002; Gong et al., 2003; Liu et al., 2003; Shao et al., 2003; Zhao et al., 2003; Reddy et al., 2004). The first simulations assimilating some aerosol information were done for INDOEX (The INDian Ocean EXperiment) by Collins et al. (2001) and Rasch et al. (2001) with the help of a chemical-transport model. In most of this second-generation prognostic aerosol models, most aerosol types were accounted for (sea salt, dust, organic and black carbon, sulphates). The package of aerosol physical parametrisations included the representation of the sources (interactive with the host model for the sea salt and dust aerosols), and of the gravitational sedimentation, dry deposition and wet deposition by precipitation together with the hygroscopicity effects on carbonaceous aerosols. The sulphur cycle was introduced (Boucher et al., 2002; Chin et al., 2002) with a simplified representation of the chemistry linking the chemical precursors to the sulphate aerosols.

Since then, a larger number of general circulation models (GCMs) have been carrying out prognostic aerosols, usually to study the sensitivity of the climate to aerosols. A survey of those, as of 2008, with details on the prognostic representation of the aerosols, details on the parametrisations in use, and comparisons of the optical properties, and radiative forcing linked to the aerosols can be found in Kinne et al. (2003, 2006), Schulz et al. (2006), and Textor et al. (2006, 2007). Regional mod-

els have also been upgraded to represent (some) aerosol processes. For example, as part of the World Meteorological Organization Sand and Dust Storm Warning and Assessment System (WMO/SDS-WAS http://www.wmo.int/sds-was), eight models (six of them regional ones) are now run pre-operationally to simulate the dust burden of the atmosphere over the European region and a number of models are now soon providing similar dust forecasts over the Asian region.

Despite the increasing number of models including prognostic aerosols, relatively few actually include an analysis of aerosol-related observations for operational weather forecasts. Such an analysis is used to define the best aerosol initial conditions to start a subsequent weather forecast including aerosol-related parameters. For example, the Chinese Meteorological Service (Zhou et al., 2008) assimilates either satellite-retrieved index of column amounts of dust aerosol or surface visibility as observed by the meteorological stations of the Chinese Meteorological Administration for their regional model. The US Naval Research Laboratory has started a full operational system mid-October 2009 (http://www.nrlmry.navy.mil/ aerosol/), which includes MODIS (MODerate resolution Imaging Spectroradiometer) observations of the aerosol optical depth at 550 nm (τ_{550} over the ocean in its analysis (Zhang et al., 2005, 2008, Zhang and Reid, 2006). The Goddard Global Modeling and Assimilation Office (GMAO) uses the Goddard Chemistry Aerosol Radiation and Transport (GOCART; Chin et al., 2002) with MODIS τ_{550} to provide an analysis of aerosol optical depth and speciation (http://gmao.gsfc.nasa.gov/research/aerosol/). Similar effort has also been reported including the assimilation of CALIPSO (Cloud-Aerosol Lidar and Infrared Pathfinder Satellite Observations) observations via a 4-dimensional Ensemble Kalman Filter approach by Sekiyama et al. (2009) for the National Institute of Environmental Studies of Japan.

Nowadays, most of the GCMs used for climate studies have included a description of aerosols and of their effects of radiation and cloud fields. If prognostic aerosols in climate GCMs are now standard features, their introduction in global weather forecast models is much more recent. The model from the European Centre for Medium-range Weather Forecasts (ECMWF) has had since the 1980s a climatological representation of the main aerosol types, first from Tanré et al. (1984), which was superseded in 2003 by climatologies derived as monthly means from chemical-transport model simulations (Tegen et al., 1997). At the time, such a change in aerosol climatologies was shown to be able to affect the meteorology both locally (Tompkins et al., 2005) and remotely through teleconnections (Rodwell and Jung, 2008).

As part of the GEMS project (Global and regional Earth-system Monitoring using Satellite and in-situ data; Hollingsworth et al., 2008), the ECMWF has developed its assimilation system to include observations pertaining to greenhouse gases, reactive gases and aerosols. In the ECMWF/GEMS configuration, the Integrated Forecast System (IFS) in the computation of the trajectory forecast used in the assimilation, has been extended to include a number of tracers, which are advected by the model dynamics and interact with the various physical processes.

ECMWF first produced a reanalysis for the years 2003 to 2008, then from July 2008 used the same experimental system for pre-operational near-real time analysis and forecast (see GEMS web address in reference). With respect to the aerosols, sources have thus been added to the model, and a representation of the aerosol physical processes (namely the interactions of the aerosols with the vertical diffusion and the convection, plus the sedimentation, dry deposition and wet deposition by large-scale and convective precipitation) are now part of the package of physical parametrisations of the ECMWF IFS model (Morcrette et al., 2009). Details of the analysis of MODIS data to constrain the initial values of the aerosols at the start of the forecasts can be found in Benedetti et al. (2009).

During GEMS, the aerosols were not interactive with either the model radiative or cloud processes, and the radiation fields were computed using the monthly mean climatological distributions of aerosol. As

part of the follow-up MACC project (Monitoring Atmospheric Composition and Climate; Simmons, 2010), the aerosol analysis and forecast system has been further developed to allow the prognostic aerosols to interact with the rest of the model. This paper discusses results obtained during the development of the improved system, particularly the impact of the prognostic aerosols on both radiation and cloud processes and how this modifies various parameters during the forecasts and how it affects standard meteorological scores.

Section 2 describes the various model configurations used in the study. Aerosol direct effect (ADE) on radiation and aerosol indirect effects (AIE) on liquid water clouds are explored in different stages. In section 3, the impact of these aerosol effects on the analysis is first studied, and the need for an analysis accounting for the various aerosol effects is addressed. In section 4, the impact on various model fields and objective scores of having the prognostic aerosols in a fully interactive way in the MACC aerosol system is then studied. Given the high cost of carrying out prognostic aerosols during the forecast, an alternative in which the analyzed aerosols are kept constant during the 10-day forecasts is studied in section 5. Conclusions and perspectives are discussed in Section 6.

2 Model description and experimental design

2.1 Description of the aerosol model parametrisations in the ECMWF IFS

A detailed description of the ECMWF forecast model including aerosol processes at the time of GEMS is given in Morcrette et al. (2009). The differences between the MACC and GEMS aerosol systems are documented in Morcrette et al. (2011).

The initial package of ECMWF physical parametrisations dedicated to aerosol processes mainly follows the aerosol treatment in the LOA/LMD-Z model (Laboratoire d'Optique Atmosphérique/Laboratoire de Météorologie Dynamique: Boucher et al., 2002, Reddy et al., 2005). Five types of tropospheric aerosols are considered: sea salt, dust, organic and black carbon, and sulphate aerosols. A prognostic representation of the stratospheric aerosols is not included here, as the impact of aerosols on radiation and cloud processes is a tropospheric feature. In the following, all results correspond to a version of the ECMWF model with prognostic tropospheric aerosols and climatological stratospheric aerosols. Similarly, the emission of aerosols by volcanoes is not present in the following results. Both types of aerosols will be considered in a later stage of the introduction of aerosols in the ECMWF IFS.

For all tropospheric aerosols, sources are defined, the sedimentation of all particles, and the wet and dry deposition processes are represented. For organic matter (OM) and black carbon (BC), two components, hydrophobic and hydrophilic, are considered, and the transfer from hydrophobic to hydrophilic is also included. The sulphur cycle is considered via a precursor variable SO_2 transformed in a sulphate aerosol (SO_4) with a time-scale simply dependent on latitude (as in Huneeus and Boucher, 2007).

A bin representation is used in this study to include prognostic aerosols of natural origin (taken to mean sea-salt SS and dust DU). The maximum flexibility regarding the limits of the bins for the sea-salt and dust aerosols is allowed in the model. In the following, the sea-salt aerosols are tentatively represented by 3 bins, with limits at 0.03, 0.5, 5 and 20 microns. Similarly, the desert dust aerosols are represented by 3 bins with limits at 0.03, 0.55, 0.9, and 20 microns. The above limits are chosen so that roughly 10, 20 and 70 percent of the total mass of each aerosol type are in the various bins.

The natural aerosols (SS, DU and dimethyl-sulphide DMS) have their sources only linked to some prognostic and diagnostic model variables. In contrast, the anthropogenic aerosols (organic matter OM, black
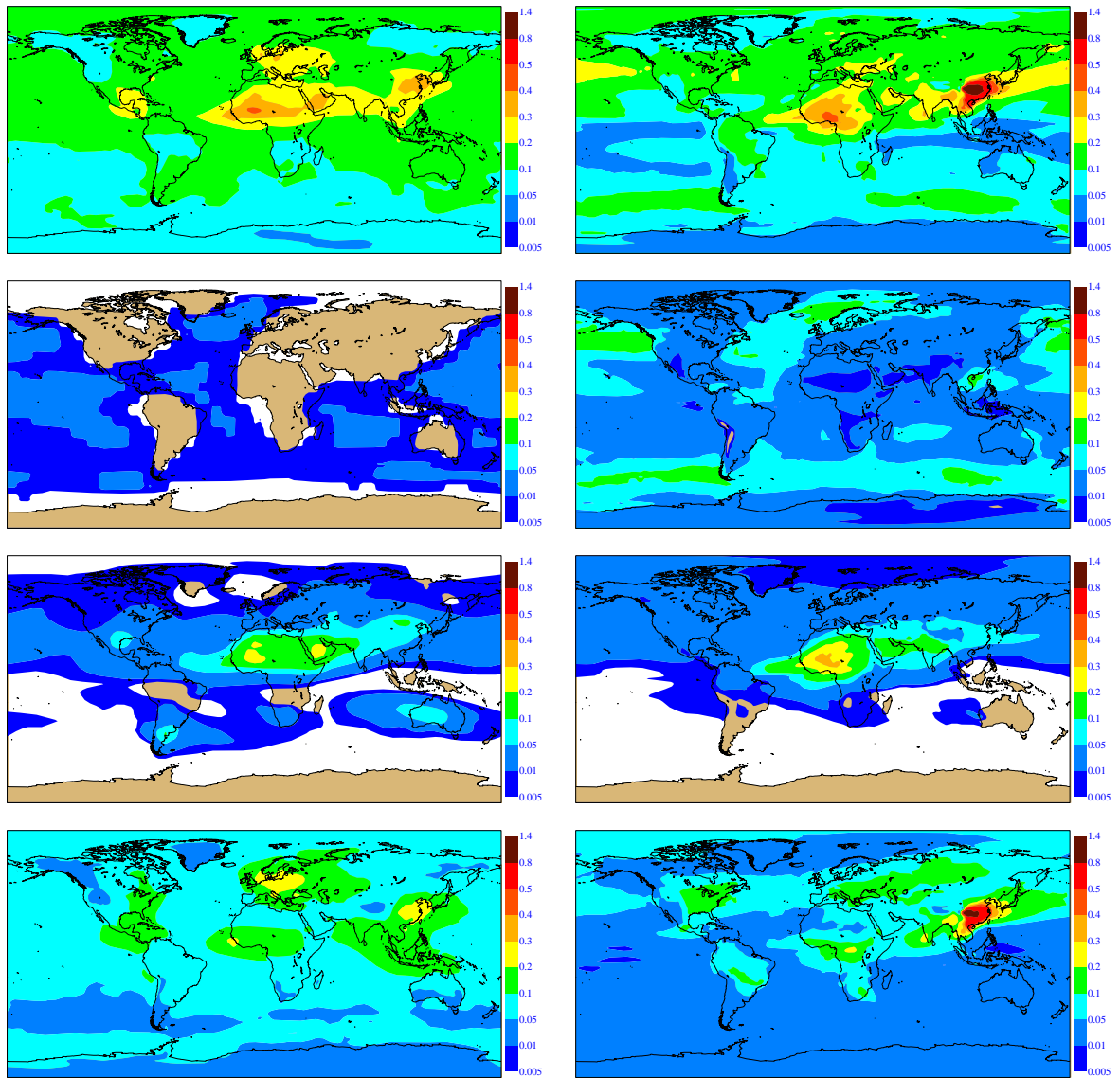
Figure 1: The climatological (left) vs. the prognostic aerosols (right) for March 2011. The optical depths of the climatological aerosols are derived from Tegen et al. (1997), whereas those for the prognostic ones correspond to the Ref configuration. From top to bottom are presented the total aerosol optical depth, the optical depth for sea-salt, dust, and anthropogenic aerosols (the sum of black and organic carbon, and sulphate aerosols).
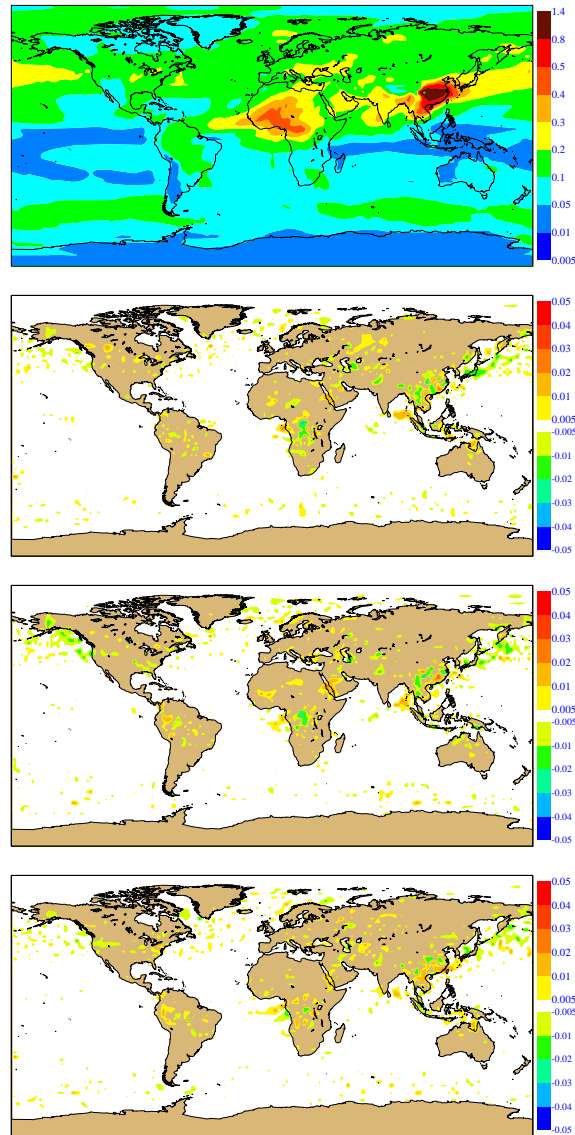
Figure 2: The analyzed total aerosol optical depth at 550 nm for March 2011 (top: Ref), and the differences FPDir-Ref, FPInd-Ref, FPDirInd-Ref in analyzed total aerosol optical depth for March 2011, all obtained with the cycle 37R2 MACC system including the relevant aerosol configuration in the analysis.

carbon BC and SO_4) have their sources read from external data-sets. Sources of sea-salt and desert dust are interactive with surface and near-surface variables of the model. Sources for the other aerosol types linked to emissions from domestic, industrial, power generation, transport and shipping activities, are taken either from the GFED (Global Fire Emission Database), SPEW (Speciated Particulate Emission Wizard), and EDGAR (Emission Database for Global Atmospheric Research) annual- or monthly-mean climatologies. More details on the sources of these aerosols are given in Dentener et al. (2006). Emissions of OM, BC and SO_2 linked to fire emissions are obtained using the analysis of MODIS and SEVIRI satellite observations by Kaiser et al. (2009, 2011).

Several types of removal processes are considered, i/ the dry deposition including the turbulent transfer to the surface, ii/ the gravitational settling, and iii/ the wet deposition including rainout (by large-scale and convective precipitation) and washout of aerosol particles in and below the clouds. The wet and dry deposition schemes are standard, whereas the sedimentation of aerosols follows closely what was introduced by Tompkins (2005) for the sedimentation of ice particles. Hygroscopic effects are also considered for organic matter and black carbon aerosols. As part of the MACC project, the analysis is run including the assimilation of MODIS aerosol optical depth at 550 nm, then is followed by a forecast in which the prognostic aerosols, although having the sources, transport, and sinks interactive with the rest of the model physics and dynamics, are not intercative with either the radiation scheme or the cloud processes. In the following, results from this set of model analyses and forecasts are referred to as Ref.

The MACC/ECMWF system used in this study uses a T_L255 L60 model version of the IFS (corresponding to a horizontal grid of around [0.70 deg]^2 and 60 vertical levels between the surface and 0.1 hPa), and the cycle 37R2 of the ECMWF libraries. For the aerosol analysis, the MACC system is based on the assimilation of MODIS Aerosol Optical Depth (AOD) at 550nm (Benedetti et al. 2009), including a definition of the observation errors fixed to values of 0.1 over land, and 0.05 over the ocean and the introduction of a variational bias correction based on the operational set-up for assimilated radiances (Dee and Uppala, 2008).

Figure 1 compares the total aerosol optical depth in the visible part (τ_{vis}) of the short-wave spectrum (440-690 nm) as derived for March, from the Tegen climatology ($Clim$) to the Ref aerosol optical depth at 550 nm (τ_{550}) for March 2011, averaged over the last five days of 10-day forecasts. Although the overall globally averaged aerosol optical depth is not very different, the details of the distribution of the different aerosol types are. The presence of sea salt aerosol in the storm track of both the Northern and Southern hemispheres is more marked in Ref than in $Clim$. The optical depth of dust is more concentrated over Sahara in Ref than in $Clim$. The overall amount of anthropogenic aerosols over the Southern hemisphere oceans is less in Ref than in $Clim$. The maximum of anthropogenic aerosols over China is much bigger in Ref than in $Clim$ ($\tau_{550} = 1.25$ vs. $\tau_{vis} = 0.28$). Compared to the climatological aerosols, the prognostic aerosols also display a much increased temporal, horizontal and vertical variability (not shown), and each of the 11 aerosol components may now directly respond to the variations in relative humidity. Finally, although both the $Clim$ and the prognostic aerosols enter the short-wave and long-wave radiation schemes in a similar way, the optical properties of the prognostic aerosols rely on much more recent observations and/or theoretical calculations than those used for establishing the $Clim$ aerosol optical properties.

2.2   Interactions between aerosols and radiation

The direct effect of the prognostic aerosols is their impact on the reflection, scattering and absorption of radiation. Instead of using the optical thicknesses defined by the aerosol climatologies, the impact is now simply introduced by computing the relevant optical thicknesses of the 11 aerosol components in the 16 (14) spectral intervals of the long-wave (short-wave) radiation scheme (Mlawer et al., 1997; Iacono et
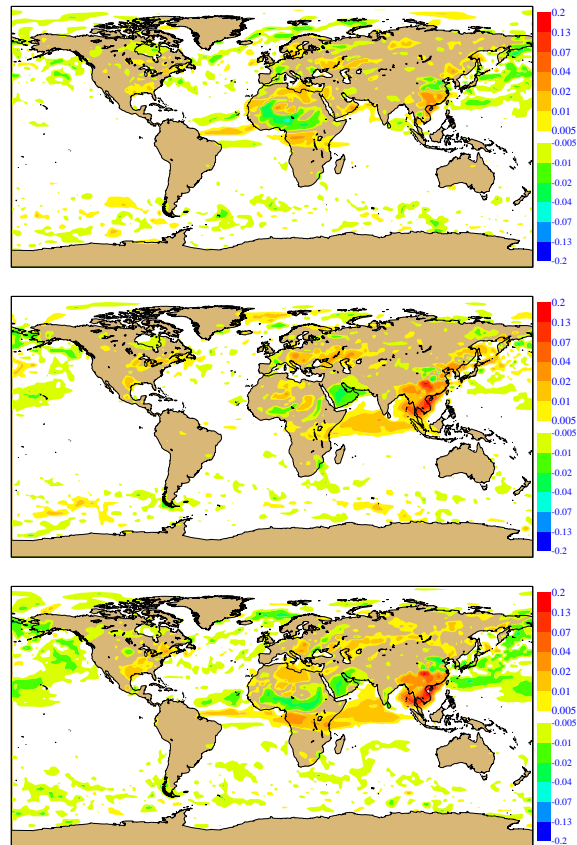
Figure 3: The difference in total aerosol optical depth at 550 nm averaged over the last five days of sets of 10-day forecasts for March 2011 obtained with the four configurations Ref, Dir, Ind and DirInd. Results are respectively FPDir-Ref, FPInd-Ref, FPDirInd-Ref (panels, from top to bottom). All forecasts start from their own analysis with the cycle 37R2 MACC system including either the Ref, FPDir, FPInd, or FPDirInd configuration. Note that the colour scale is different from the one in Fig. 2.

al., 2004; Morcrette et al., 2008). These aerosol optical thicknesses are added to the optical thicknesses due to the radiatively active gases and those of the clouds if present.

The refractive indices were derived from Lacis (2001) for sea salt and interpolated from Dubovik et al. (2002) for desert dust. Then a standard Mie scattering algorithm (Ackerman and Toon, 1981) is applied using, for sea salt and dust aerosols, the particle size distribution as simulated by the bin scheme but also accounting for a fixed size distribution within each bin that has been calibrated against a model with more bins. Optical depth for sea salt and dust are obtained by summing the individual bin contributions (assumed to be independent in the bin representation used for the ECMWF IFS) to the optical thickness for each aerosol type. Absorption and scattering coefficients for organic and black carbon, and sulphate were adapted from those in the LOA/LMD-Z model (see Table 2 in Reddy et al., 2005) and are based on Hess et al. (1998). Sea-salt and sulphate aerosols have their optical properties depending on the local relative humidity with the relevant growth factor taken from Tang (1997) and Tang and Munkelwitz (1994), respectively. In the absence of reliable data for *OM*, the same growth factor as for SO_4 is used for *OM* (Reddy et al., 2005).
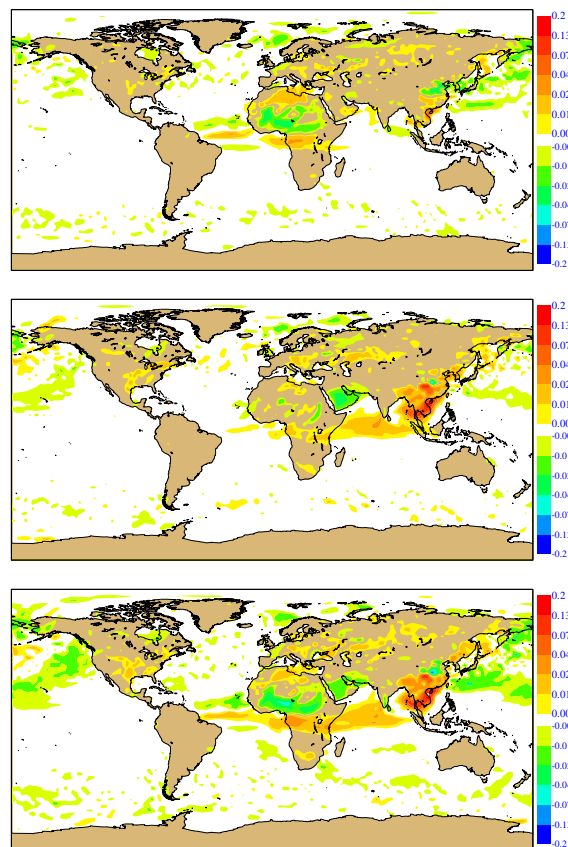
Figure 4: As in Figure 3, but the FP_RDir, FP_RInd, and $FP_RDirIndir$ forecasts all start from the Ref analysis with the cycle 37R2 MACC system. Same colour scales as in Fig. 3.

2.3 Interactions between aerosol and cloud processes

In the following, the indirect aerosol effects are addressed following the nomenclature of Lohmann and Feichter (2005), affecting both liquid water and ice clouds.
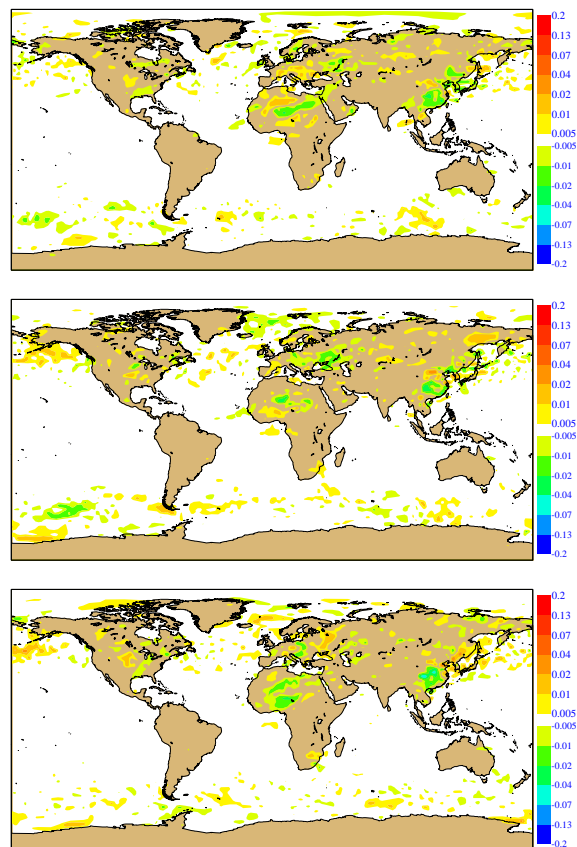
Figure 5: The difference in total aerosol optical depth at 550 nm averaged over the last five days of 10-day forecasts for March 2011. For each configuration, Dir, Ind, or DirInd (top to bottom), the differences are shown for the forecasts starting either from the dedicated or the Ref analysis (see text). Same colour scales as in Fig. 3.

2.3.1 Liquid water clouds

For liquid water clouds, the following indirect effects are included, the so-called first indirect or Twomey effect (Twomey, 1974) where more numerous smaller cloud particles reflect more solar radiation (through enhanced scattering) and decrease the precipitation efficiency thereby prolonging cloud lifetime. The first indirect effect, i.e., the impact of the aerosols likely to act as cloud condensation nuclei is introduced following Menon et al. (2002). The mass corresponding to the first bin of sea salt, hygrophilic organic carbon aerosol, and sulphate aerosols is used to provide a diagnostic of the number N_{CCN} of cloud condensation nuclei

$$N_{CCN} = 10^{2.41 + 0.13 log_{10}(m_{OM}) + 0.05 log_{10}(m_{SS}) + 0.50 log_{10}(m_{SO_4})} \qquad (1)$$

where m_x are the mass concentrations (in $\mu g/m^3$), and r_x are the coefficients for OM, SS and SO_4 as derived from a regression analysis by Menon et al. (2002). N_{CCN} is then used in the calculation of the effective radius of the liquid water cloud droplets, using the framework of Martin et al. (1994).

This N_{CCN} is also used for computing critical mixing ratios for autoconversion (of warm rain) following Rotstayn and Penner (2001), which are then used for large scale and convective precipitation. The rain autoconversion and cloud collection by rain droplets originating from either large-scale or convective precipitation follows Sundqvist (1988) and Sundqvist et al. (1989), assuming a critical droplet radius of 9.3 μm, and allowing the cloud water content to vary between 0.1 and 10 times a critical cloud water content set to $3x10^{-4}$ gm^{-3}.

The semi-direct effect (linked to the absorption of solar radiation by black carbon) is present by default in the model as the increased heating may cause evaporation of cloud particles. However, this is not included as an interaction between aerosol, heating rate and cloud water built-in within the cloud scheme. It may occur via the model time evolution of the black carbon aerosol, temperature, cloud liquid water and evaporation.

2.3.2 Ice clouds

Please note that at this stage, the indirect effects of aerosols on ice clouds are not included, as there still appears to be much debate on which aerosols and under which mixing assumptions these aerosols might contribute to the number of ice nuclei (IN) and possibly modulate ice content of high-level and/or mixed-phase clouds (Lohmann and Feichter, 2001; Lohmann, 2002; Lohmann and Kärcher, 2002; Spichtinger and Gierens, 2009; Lee and Penner, 2010).

Hereafter, results including the aerosol direct effect are referred to as *Dir*, those with just the aerosol effects on the CCNs and autoconversion rate for warm rain, as *Ind*, and results including both the direct and indirect effects are referred to as *DirInd*. Note that the exact name of the configuration will depend on whether it uses fully prognostic aerosols starting from a dedicated analysis with fully prognostic aerosols (*FP...*), or a similar configuration starting from the *Ref* analysis, thereafter referred to as *FP_R...*. In section 5, configurations run with analyzed aerosols then fixed during the forecasts will be referred to as *AF...*.
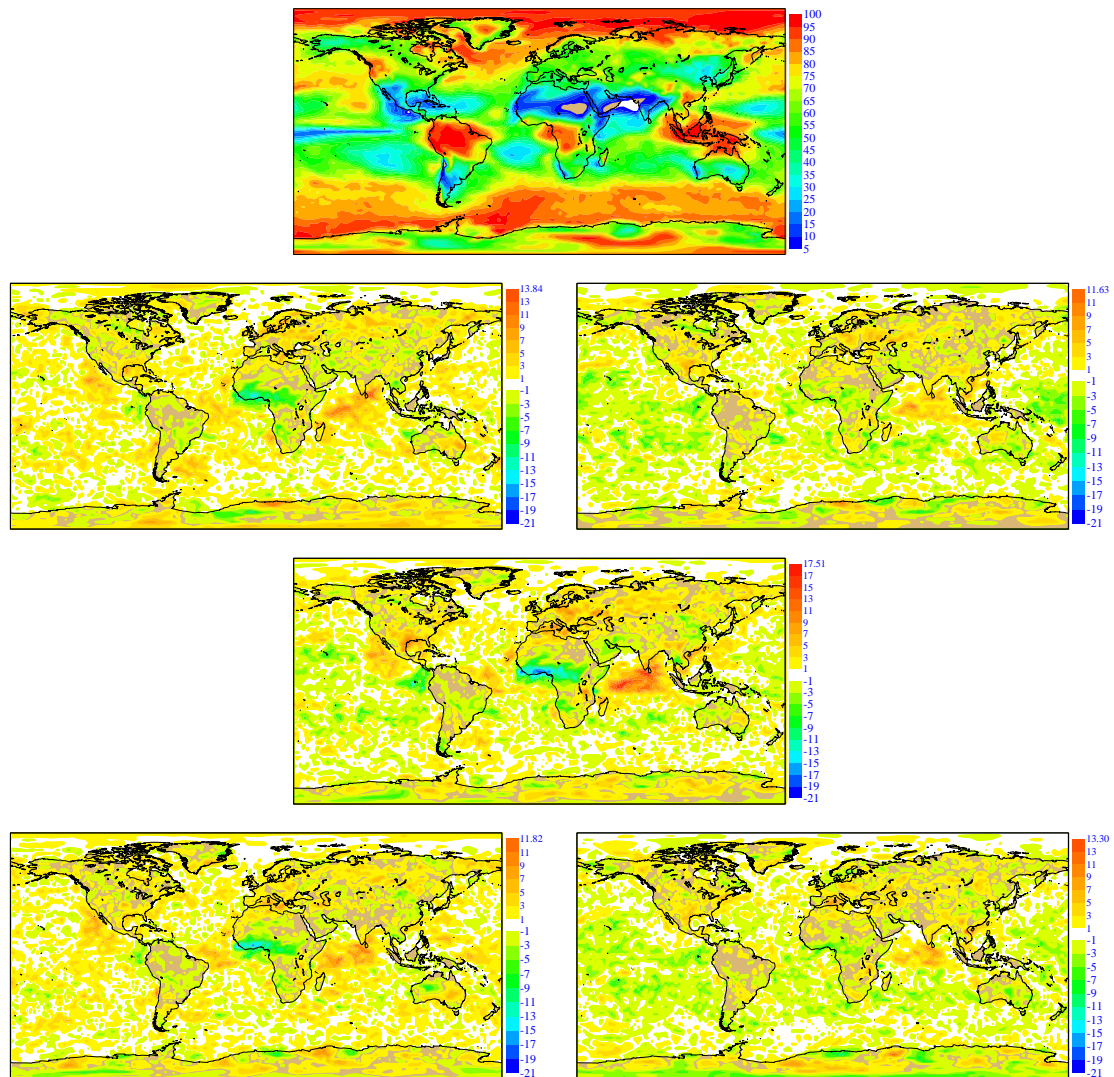
Figure 6: The monthly average over the last five days of 10-day forecasts of the differences FPDir-Ref (top left), FPInd-Ref (top right), FPDirInd-Ref (middle) for the total cloudiness (in percent) for March 2011. The two bottom figures are the differences FPDirInd-FPInd (bottom left) and FPDirInd-FPDir (bottom right) in the same conditions. All forecasts start for the relevant Ref, Dir, Ind, or DirInd analysis.
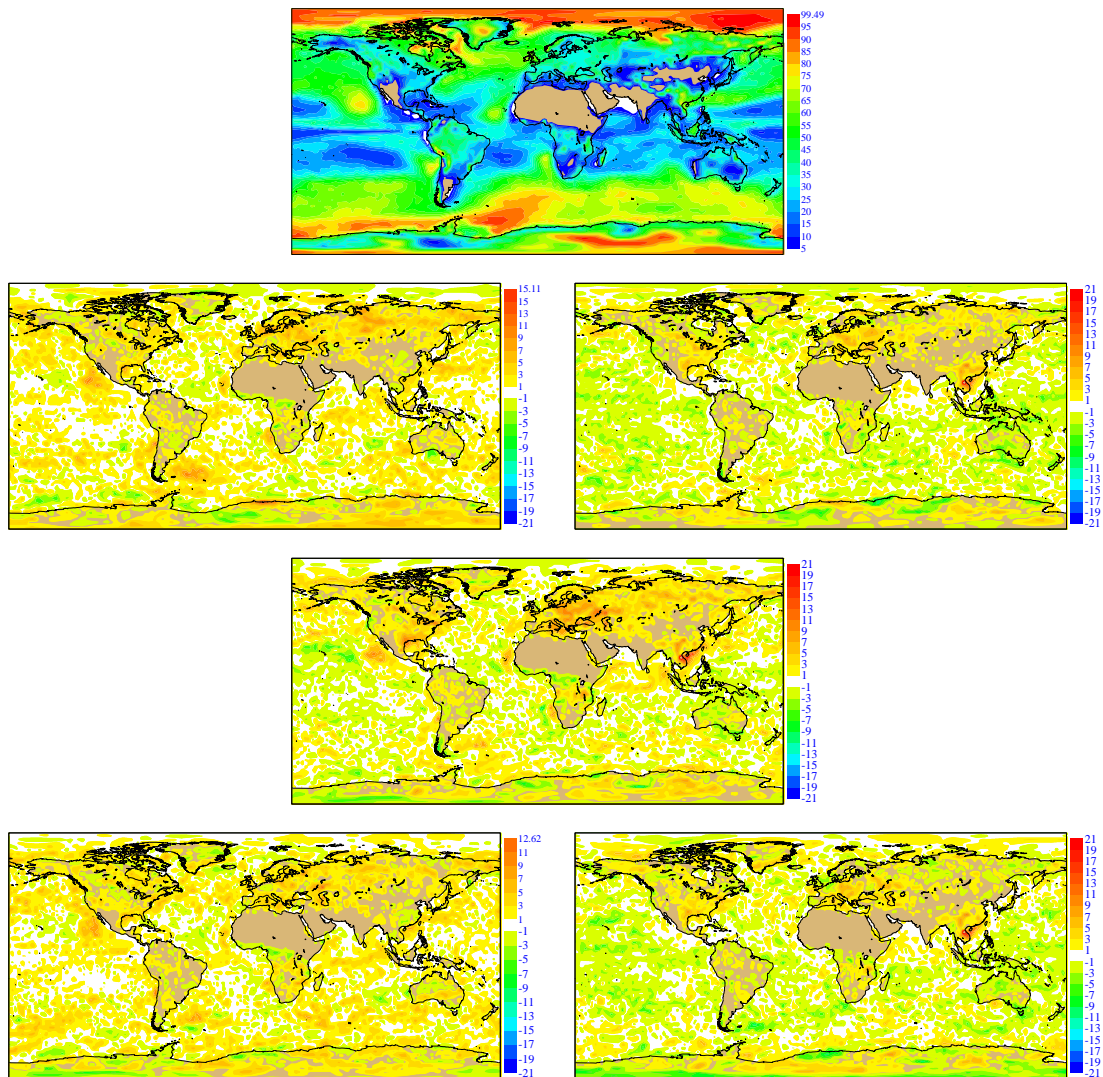
Figure 7: The monthly average over the last five days of 10-day forecasts of the differences FPDir-Ref (top left), FPInd-Ref (top right), FPDirInd-Ref (middle) for the low-level cloudiness (in percent) for March 2011. The two bottom figures are the differences FPDirInd-FPInd (bottom left) and FPDirInd-FPDir (bottom right) in the same conditions. All forecasts start for the relevant Ref, Dir, Ind, or DirInd analysis. Same colour scales as in Fig. 6.
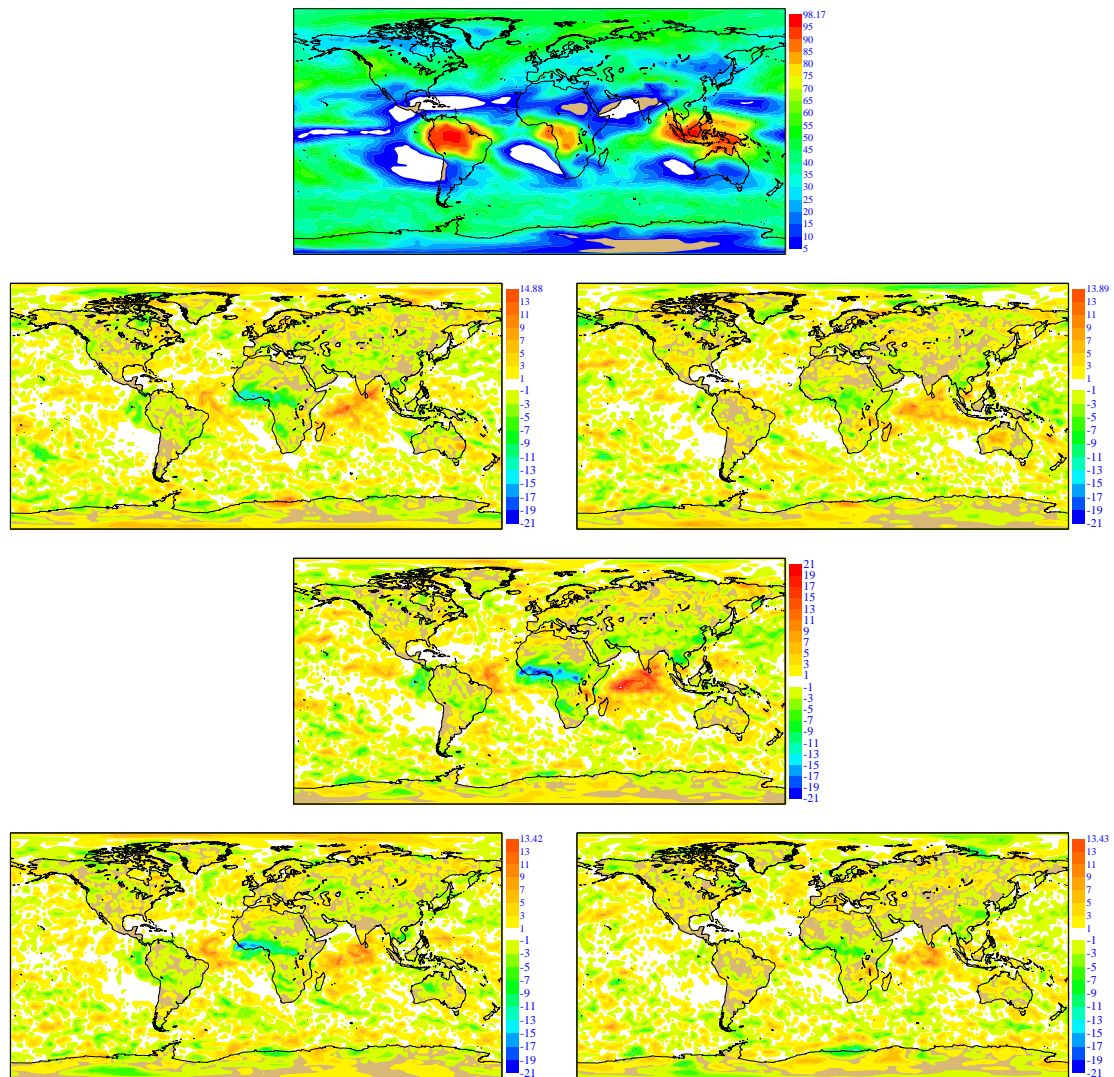
Figure 8: The monthly average over the last five days of 10-day forecasts of the differences FPDir-Ref (top left), FPInd-Ref (top right), FPDirInd-Ref (middle) for the high-level cloudiness (in percent) for March 2011. The two bottom figures are the differences FPDirInd-FPInd (bottom left) and FPDirInd-FPDir (bottom right) in the same conditions. All forecasts start for the relevant Ref, Dir, Ind, or DirInd analysis. Same colour scales as in Fig. 6.

3 Impact of representing Dir, Ind, and $DirInd$ on the analysis

In the GEMS aerosol analysis and forecast system, the prognostic aerosols were kept completely passive with respect to radiation and cloud processes, making them quantities originating from sources, being horizontally and vertically advected by the model dynamics and vertical diffusion and convection, being deposited by sedimentation and wet deposition. The MACC system retained this configuration (hereafter called Ref) and added three more, with 1/ only the direct effect on radiation being included, as described in section 2.2, 2/ only the indirect effects on liquid water cloud effective radius and precipitation efficiency being included, as described in section 2.3.1., and 3/ the combination of these direct and indirect effects ($DirInd$).

In the following, these last configurations with fully prognostic (FP) aerosols in both the analysis and the forecasts are referred to as $FPDir$, $FPInd$, and $FPDirInd$. The reference system when the prognostic aerosols are used in the analysis, but the prognostic aerosols are not interactive with either radiation or cloud processes is referred to as Ref.

Five weeks of analysis have been run with these four different configurations between 23 February and 31 March 2011. Note that, prior to 23 February 2011, the GEMS/MACC analysis system (including the analysis of aerosols assimilating MODIS optical depth at 550 nm) had been carrying a Ref-type analysis of aerosols since September 2008 in near-real time. Figure 2 presents, averaged over the month of March 2011, the Ref τ_{550}, and the differences $FPDir - Ref$, $FPInd - Ref$, and $FPDirInd - Ref$. The impact on the aerosol analysis of the interactions with radiation and/or cloud processes is rather small, with maximum absolute difference in τ_{550} of 0.03. This small effect is a direct consequence of the way the aerosol analysis is performed. The MODIS τ_{550} is assimilated and the agreement between model and MODIS-derived τ_{550} is improved, but the aerosol analysis does not feed back on the analysis of the other meteorological parameters, so the primary fields of temperature, humidity and winds are only driven by the numerous other observations ingested during the assimilation. The impact of the different configurations of aerosols can only be felt via the potential changes to the 12-hour forecast used as the trajectory around which the analysis is performed.

4 Impact of fully interactive prognostic aerosols on the 10-day forecasts

At this stage, the first question is simply: Is a consistent analysis including the aerosol effects required for providing a reasonable representation of the aerosol effects in the subsequent forecasts? or could one do away with an aerosol analysis, similar to the Ref one where aerosols are not interactive with the rest of the model, and then run the various configurations $FPDir$, $FPInd$, $FPDirInd$ all starting from the Ref analysis. The answer to this question might be of interest to the community likely to run their forecasts from aerosol analyses provided by ECMWF.

4.1 Aerosol optical depth

Figure 3 presents the differences in τ_{550}, respectively $FPDir$-Ref, $FPInd$-Ref, $FPDirInd$-Ref, when all forecast are started from their respective analysis, namely $FPDir$ forecast from $FPDir$ analysis, $FPInd$ forecast from $FPInd$ analysis, $FPDirInd$ forecast from $FPDirInd$ analysis. Results are presented as a monthly mean for March 2011 for the average τ_{550} in the last five days of the subsequent 10-day forecasts, for all four configurations. From Figure 3, it is clear that even if the analyses were displaying relatively small differences in initial aerosol conditions, the differences in treatment of the interactions

of the aerosols with either the radiation and/or the clouds make the aerosol distributions diverge more over the length of the forecasts. Figure 3 shows that relatively speaking the direct and indirect effects of aerosols is roughly linear: The bottom panel of Figure 3 (*FPDirInd-Ref*) is generally related to the sum of features, positive or negative, in the top panel (*FPDir-Ref*) and the middle panel (*FPInd-Ref*). This can clearly be seen over the tropical Atlantic ocean, the Indian ocean, over China, Northwest Pacific, less clearly over Africa.

Figure 4 presents the differences in τ_{550}, respectively FP_RDir-*Ref*, FP_RInd-*Ref*, *FPRDirInd-Ref*, but when all forecasts are started from the *Ref* analyses, instead of their own. Comparing Figures 3 and 4 shows that, not surprisingly the additivity of the direct and indirect effects is again visible when the forecasts are all started from the Ref analysis. The overall response of the model to the representation of the direct and indirect effects of aerosols is clearly driven by the model parametrisations and not the details of the aerosol initial conditions. Here again, it has to be emphasized that this might be due to the way the aerosol analysis is performed in the MACC system, with practically no feedback of the prognostic aerosols on the analyses, apart from their role in the individual 12-hour trajectory forecasts.

Figure 5 presents the differences in τ_{550}, for the pair of sets of forecasts with *Dir*, *Ind*, *DirInd* aerosol effects between those starting from their own analyses and those starting from the Ref analyses, typically showing the differences between Figures 3 and 4. Figure 5 can be thought to indicate the geographical areas more particularly sensitive to the details of the initial analyses given a particular representation of the direct and indirect effects. China, Sahara and some limited areas within the storm track of both hemispheres appear to be the most sensitive areas.

So the answer to the question set at the beginning of section 4 is that, with the present configuration of the MACC aerosol system, a dedicated aerosol analysis including all the details of the interactions between aerosols, radiation, and cloud processes is not strictly required to be able to give reasonable subsequent forecasts of aerosols and associated fields. In the following, results for other fields from the *Ref*, *FPDir*, *FPInd*, *FPDirInd* sets of forecasts starting from the dedicated analyses are discussed.

4.2 Cloudiness

Figure 6 presents the total cloudiness averaged over March 2011, from the last five days of sets of 10-day forecasts, starting from the *Ref* analysis, and the corresponding differences *FPDir-Ref*, *FPInd-Ref*, *FPDirInd-Ref*, *FPDirInd-FPInd* and *FPDirInd-FPDir*. The main signal within the tropical band is the decrease in cloudiness over Africa, and the increase over the Indian ocean, mainly driven by the aerosol direct effect. This is likely linked to a displacement of the centres of convection, due to a difference in the atmospheric stability over land and ocean, when either the radiative heating profiles from climatological or prognostic aerosols are considered.

The aerosol direct effect (ADE, as seen in *FPDir-Ref* or *FPDirInd-FPInd*) also leads to increase in cloudiness over most of the oceanic areas, whereas the aerosol indirect effect (AIE, as seen in *FPInd-Ref* or *FPDirInd-FPDir*) gives an overall decrease in oceanic cloudiness.

Similar plots are given in Figures 7 and 8 for low-level and high-level cloudiness respectively. In the ECMWF model, low-level cloudiness is diagnosed as cloudiness between surface and $\eta = 0.8$, whereas high-level cloudiness is diagnosed as cloudiness appearing at *eta*-levels between 0.45 and the top of the atmosphere (TOA). From Figures 7 and 8, the increase in oceanic cloudiness with ADE mainly occurs through the low-level cloudiness, as does the decrease in oceanic cloudiness with AIE. The increase in low-level oceanic cloudiness with ADE is visible in areas of stratiform clouds (off-coast California and Namibia). The decrease in oceanic cloudiness with AIE also occurs through the low-level cloudiness.
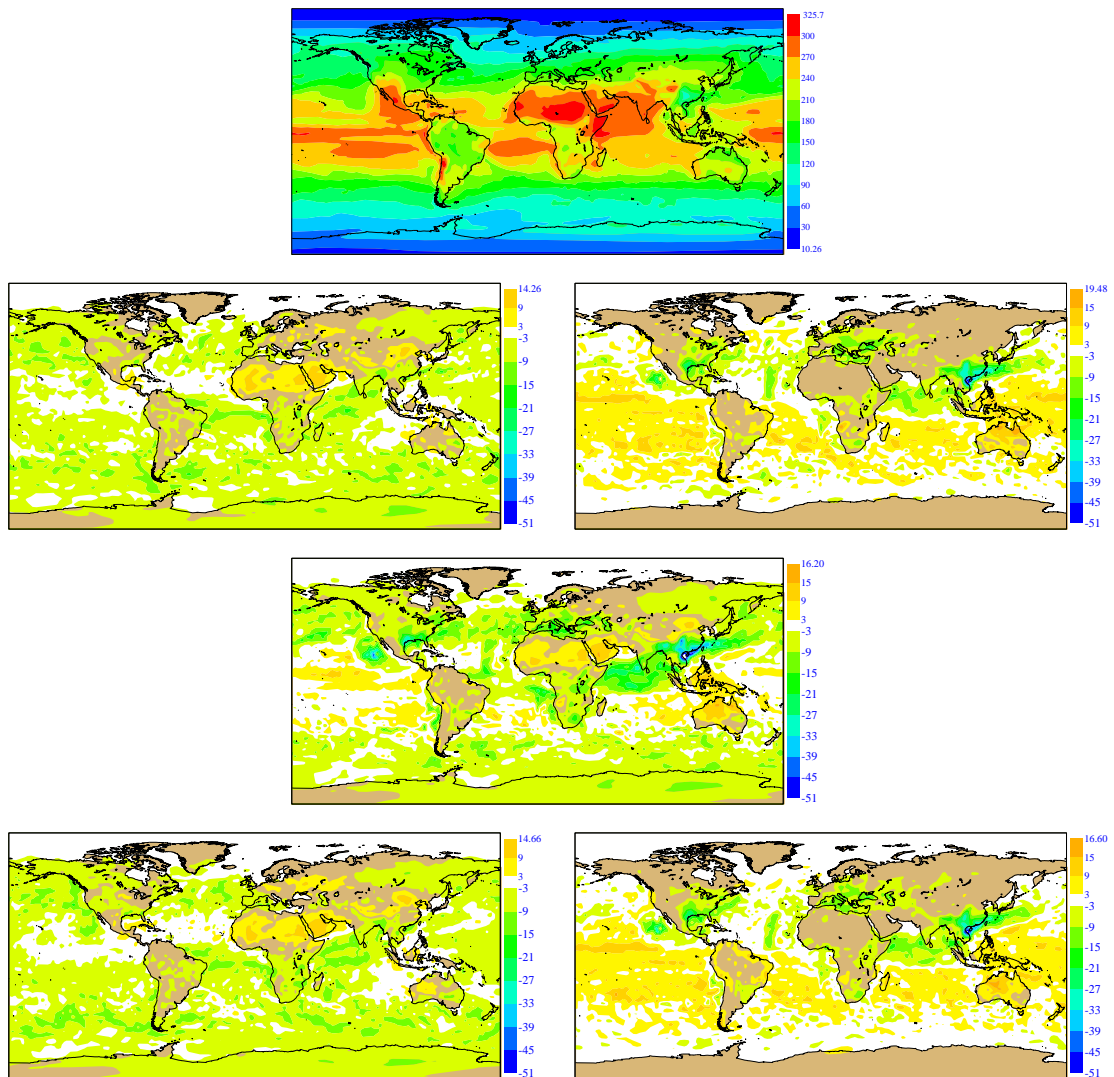
Figure 9: The monthly average over the last five days of 10-day forecasts of the differences FPDir-Ref (top left), FPInd-Ref (top right), FPDirInd-Ref (middle) in downward shortwave radiation at the surface (in Wm^{-2}) for March 2011. The two bottom figures are the differences FPDirInd-FPInd (bottom left) and FPDirInd-FPDir (bottom right) in the same conditions. All forecasts start for the relevant Ref, Dir, Ind, or DirInd analysis.
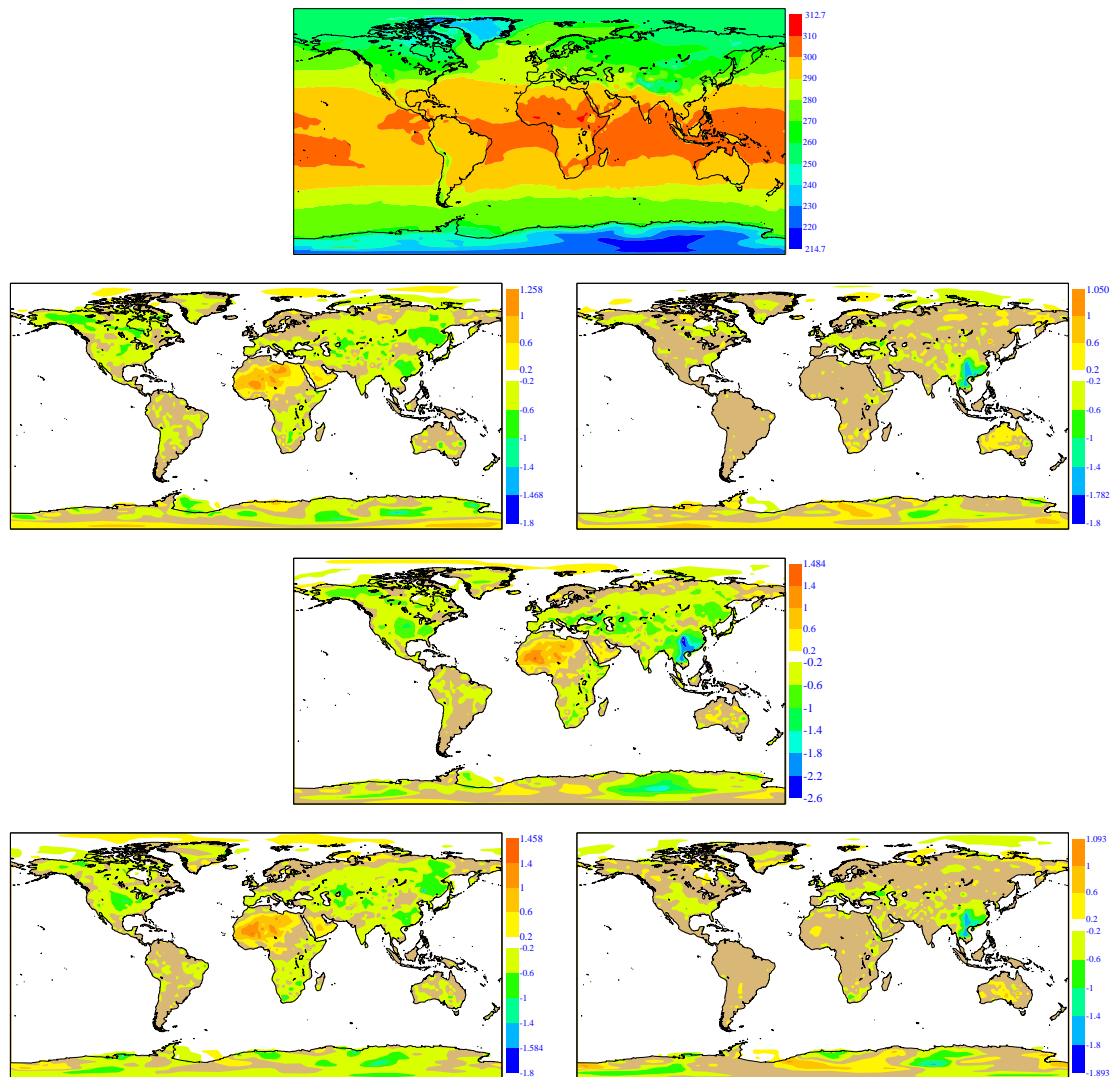
Figure 10: The monthly average over the last five days of 10-day forecasts of the differences FPDir-Ref (top left), FPInd-Ref (top right), FPDirInd-Ref (middle) for the surface skin temperature (in K) for March 2011. The two bottom figures are the differences FPDirInd-FPInd (bottom left) and FPDirInd-FPDir (bottom right) in the same conditions. All forecasts start for the relevant Ref, Dir, Ind, or DirInd analysis.
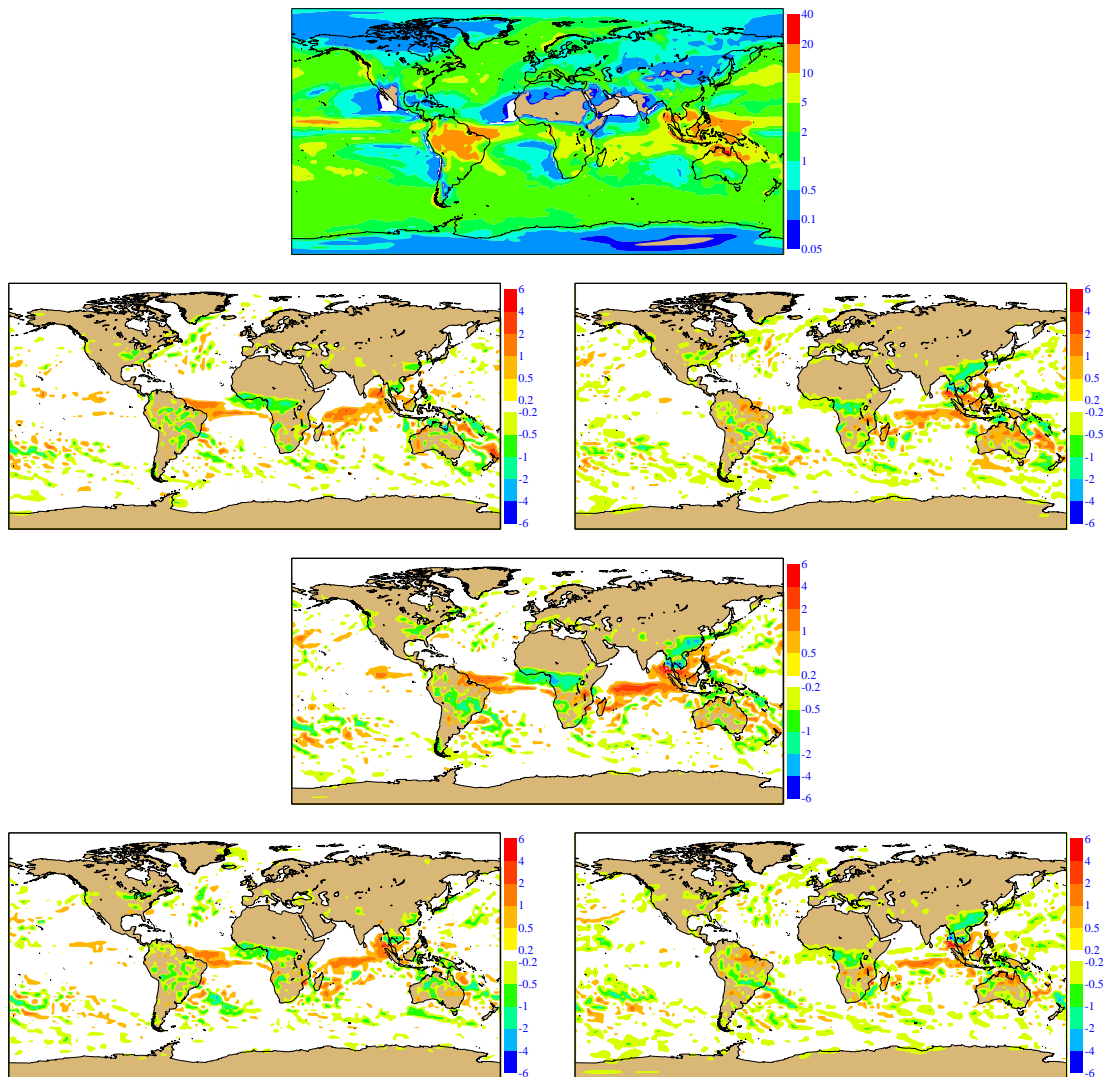
Figure 11: The monthly average over the last five days of 10-day forecasts of the differences FPDir-Ref (top left), FPInd-Ref (top right), FPDirInd-Ref (middle) for the total precipitation (in mmday^{-1}) for March 2011. The two bottom figures are the differences FPDirInd-FPInd (bottom left) and FPDirInd-FPDir (bottom right) in the same conditions. All forecasts start for the relevant Ref, Dir, Ind, or DirInd analysis.

Over the Northern hemisphere continents, both ADE and AIE give rise to increased low-level cloudiness, with the bigger contribution linked to ADE. AIE also is responsible for the increase low-level cloudiness over the Indochinese area.

As seen comparing Figures 6 and 8, the largest tropical signals seen in total cloudiness (over Africa, the Indian ocean, and west off-coast Equator/Columbia) come from the changes in high-level cloudiness. The decrease of high-level cloudiness appears to be dominated by the ADE, with a smaller contribution of the same sign by AIE, as does the increase of high-level cloudiness over the Indian ocean.

Interestingly, over the Indochinese peninsula, the high-level cloudiness shows a decrease, with contributions from both ADE and AIE.

4.3 Surface radiation, temperature and precipitation

When considering the aerosol impact of aerosols on the surface radiation budget, both the long-wave and short-wave radiative effects should be considered. However, although both the aerosol effects in the two parts of the radiative spectrum have been considered in this study, the short-wave effect clearly dominates, particularly when considering the modulation of the surface radiation budget.

4.3.1 Surface short-wave radiation

The impact of prognostic aerosols on the surface short-wave radiation differs markedly, whether the ADE or the AIE is considered. In Figure 9, the ADE gives an increase of the surface downward short-wave radiation (SSRD) over the Sahara and Arabian peninsula, showing the reduced aerosol optical depth of the prognostic aerosols related to the climatological ones, in areas where clear-sky situations are dominant. This reduction is linked to both a small decrease in the aerosol amount, when averaged over a month, compared to the quasi-static climatological aerosols (interpolated daily from monthly mean values, derived from Tegen et al., 1997), and a decrease in the extinction parameters for dust, as the dust optical properties of the MACC aerosols (Dubovik et al., 2002) is smaller than the dust optical properties implicitly included in the operational dust optical depth (computed from Hess et al., 1998).

Elsewhere where cloudiness is playing a role, ADE (in $FPDir-Ref$) also gives a decrease in SSRD over most of the rest of the globe. On the contrary, AIE in $FPInd-Ref$ gives an increased in SSRD over the tropical and Southern hemisphere oceans, with the exception of the Indian ocean, consistent with the patterns seen for cloudiness. Considering the changes in low-level and high-level cloudiness, $FPDirInd-Ref$ combines both $FPDir-Ref$ and $FPInd-Ref$ effects, keeps an increase in SSRD over Sahara, Saudi Arabia, Central Pacific and South Indian ocean, but shows a strong decrease in SSRD (in excess of 20 Wm^{-2}) over China, and the Northern Indian ocean, and smaller decrease in SSRD over North America, North Atlantic ocean, Europe, and Siberia.

4.3.2 Surface temperature

The pattern seen for the change in SSRD (albeit somewhat modulated by the much smaller change in downward change in surface downward long-wave radiation, not shown) translates roughly into the pattern seen for the change in surface temperature (Figure 10), with the ADE leading to a warming of the desert areas, and a general cooling elsewhere (North America, Eurasia). The AIE adds up some more cooling over China, and the $FPDirInd-Ref$ shows an overall cooling of the continental surfaces with the
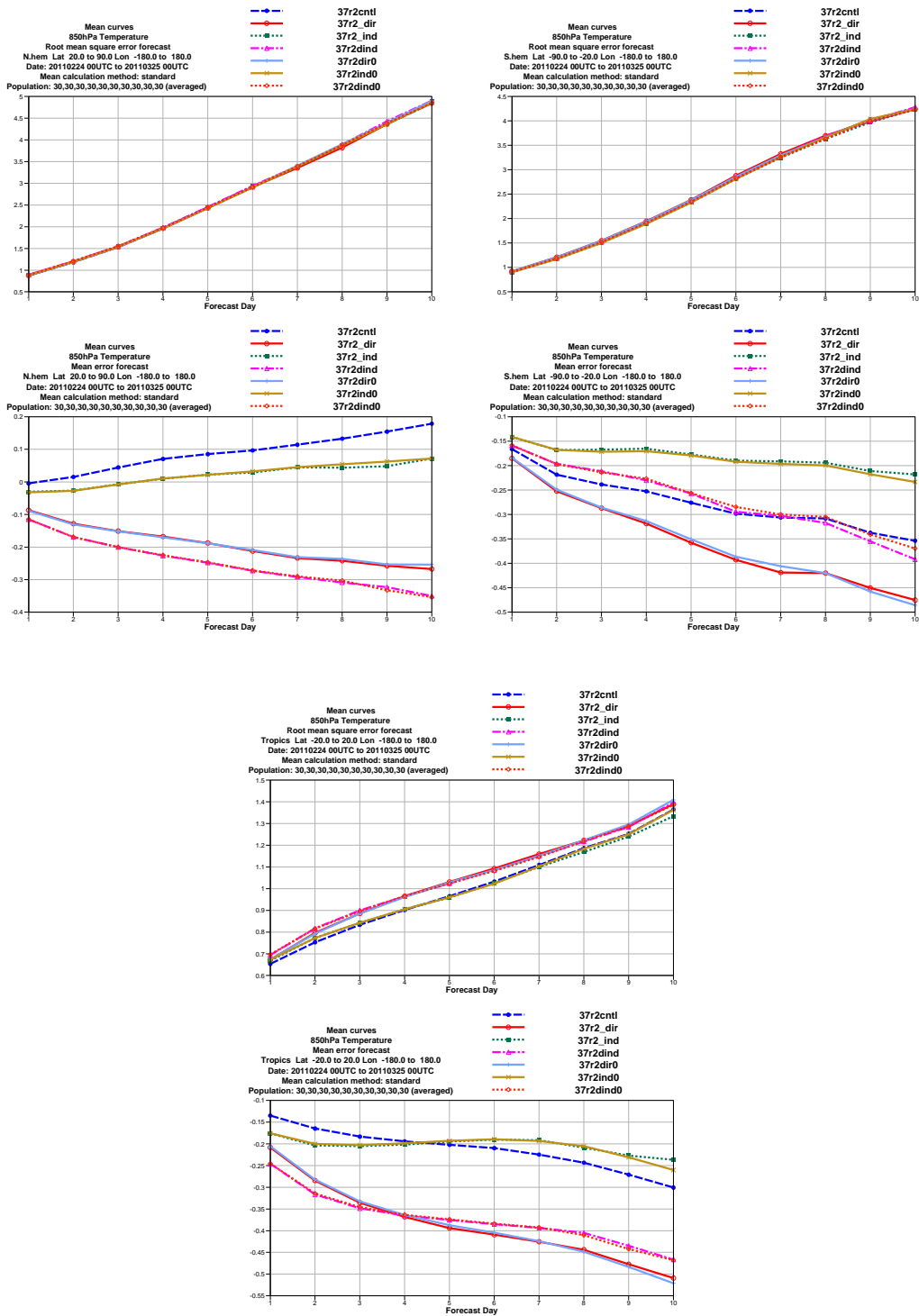
Figure 12: The root mean square error and the mean error of the temperature at 850 hPa for the forecasts for March 2011, for the Northern (two plots on the left), the Southern hemisphere (top plots on the right), and the tropical area (two plots lower down in the middle). For each set of plots, the r.m.s. error plot is on top and the mean error plot is at the bottom. For the forecasts starting with dedicated analyses, the curves correspond to Ref (blue), FPDir (red), FPInd (green), and FPDirInd (purple). For the forecasts starting from the Ref analysis, the curves correspond to $FP_R Dir$ (blue grey), $FP_R Ind$ (brown), and $FP_R DirInd$ (orange).

exception of the Sahara and the Arabian peninsula.

4.3.3 Precipitation

The impact on precipitation, here considered as the sum of the large-scale and convective precipitation, is both simpler in its distribution patterns, and more complex to explain. For the fields discussed in the previous sections, the signal seen for *FPDirInd-Ref* can generally be explained as a sum of the *FPDir-Ref* and *FPInd-Ref*, a rough addition of aerosol direct and indirect effects. For precipitation (Figure 11), the patterns of change are very much common for *FPDir* and *FPInd*, with a decrease in precipitation over African InterTropical Convergence Zone (ITCZ), a smaller but consistent decrease in precipitation over the South Pacific, mid-South America, South Atlantic, South-East of Indonesia, but an increase over the Indian ocean. Specific to ADE is the increase over the equatorial Atlantic ocean, whereas the decrease over China appears linked to the AIE.
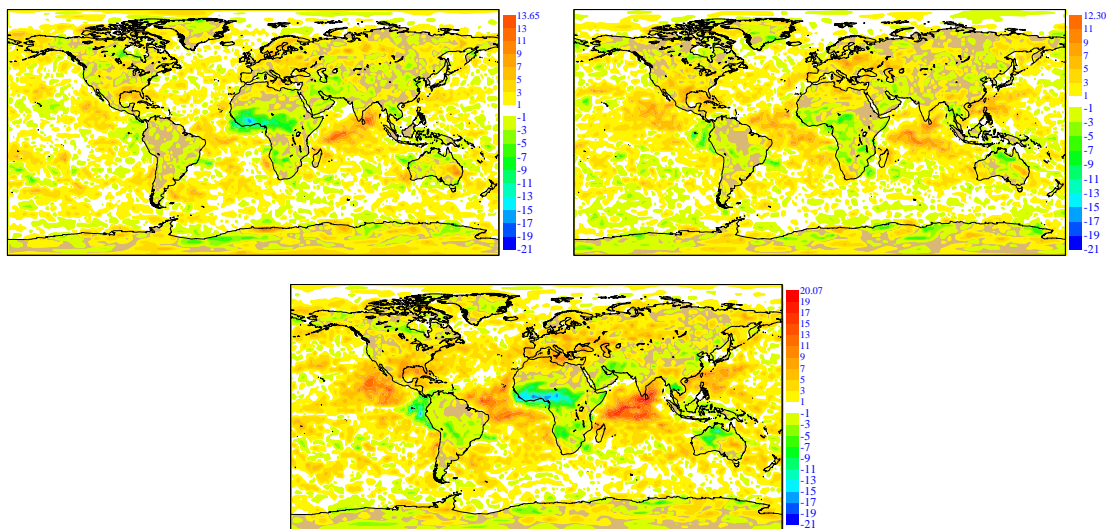
Figure 13: The monthly average over the last five days of 10-day forecasts of the differences AFDir-Ref (top left), AFInd-Ref (top right), AFDirInd-Ref (middle) for the total cloudiness (in percent) for March 2011, for forecasts using the relevant analyzed aerosols in their initial conditions, but keeping them fixed afterwards.

4.4 Objective scores

Comparisons of the standard objective scores for anomaly correlation of the geopotential at 1000 and 500 hPa, root mean square and mean error of temperature and wind at 850, 500, 200 hPa were produced for the Northern and Southern hemispheres (20°-pole), the tropical area (20^oN-20^oS), and various areas (Europe, North America, South America, Africa, North Asia, South-East Asia) for the various configurations *Ref*, *Dir*, *Ind* and *DirInd*, with the last three starting either from their dedicated sets of analyses (i.e., the *FP...* configuration), or from the *Ref* set of analyses (i.e., the FP_R... configuration).

Only the mean error of temperature in the lowest levels of the atmosphere (850 and 700 hPa) displays any significant sensitivity to the representation of interactions of the aerosols with either the radiation and/or the cloud fields. The anomaly correlation of the geopotential does not display any significant sensitivity. In Figure 12, only the root mean square error and mean error of temperature at 850 hPa for
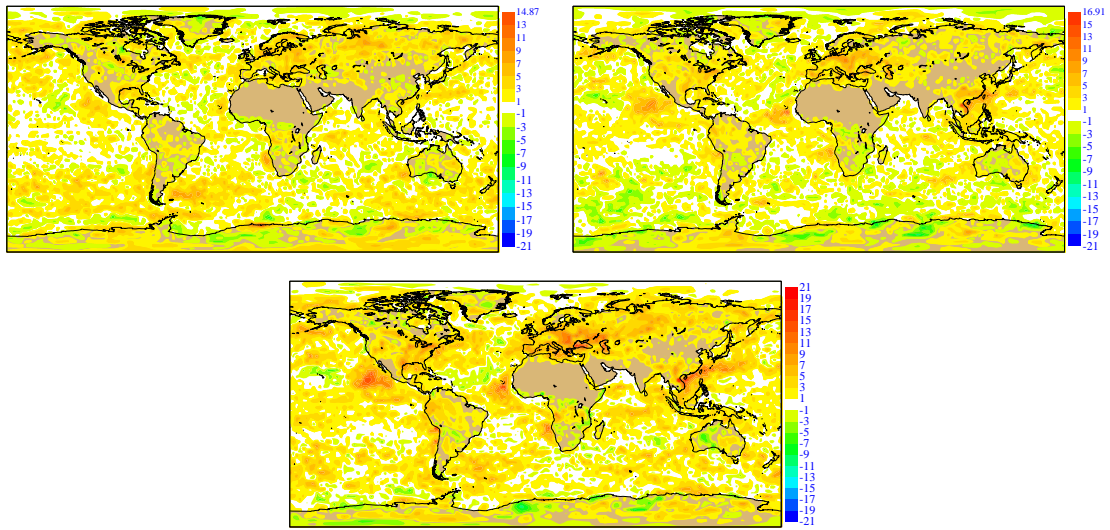
Figure 14: The monthly average over the last five days of 10-day forecasts of the differences AFDir-Ref (top left), AFInd-Ref (top right), AFDirInd-Ref (middle) for the low-level cloudiness (in percent) for March 2011, for forecasts using the relevant analyzed aerosols in their initial conditions, but keeping them fixed afterwards.
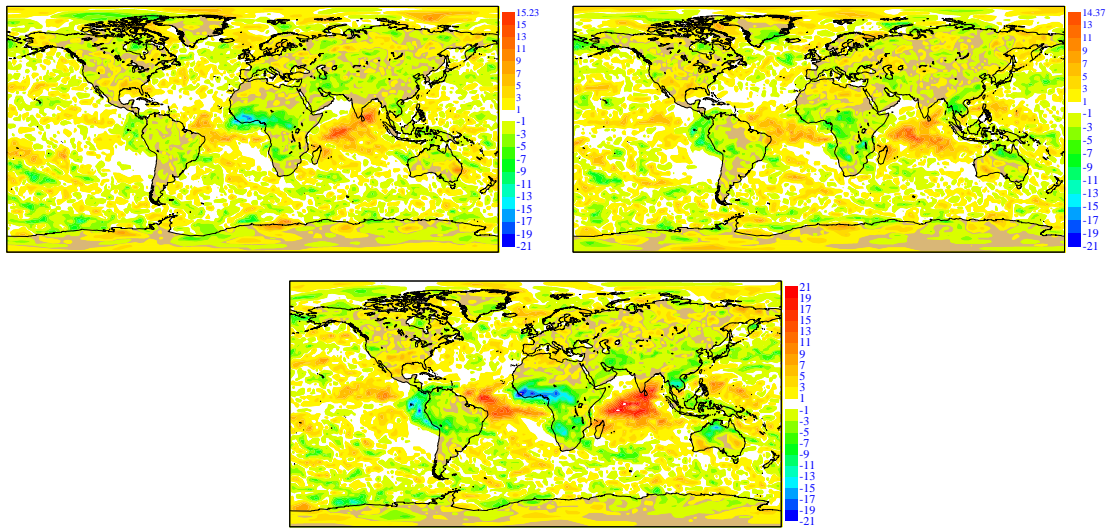
Figure 15: The monthly average over the last five days of 10-day forecasts of the differences AFDir-Ref (top left), AFInd-Ref (top right), AFDirInd-Ref (middle) for the high-level cloudiness (in percent) for March 2011, for forecasts using the relevant analyzed aerosols in their initial conditions, but keeping them fixed afterwards.
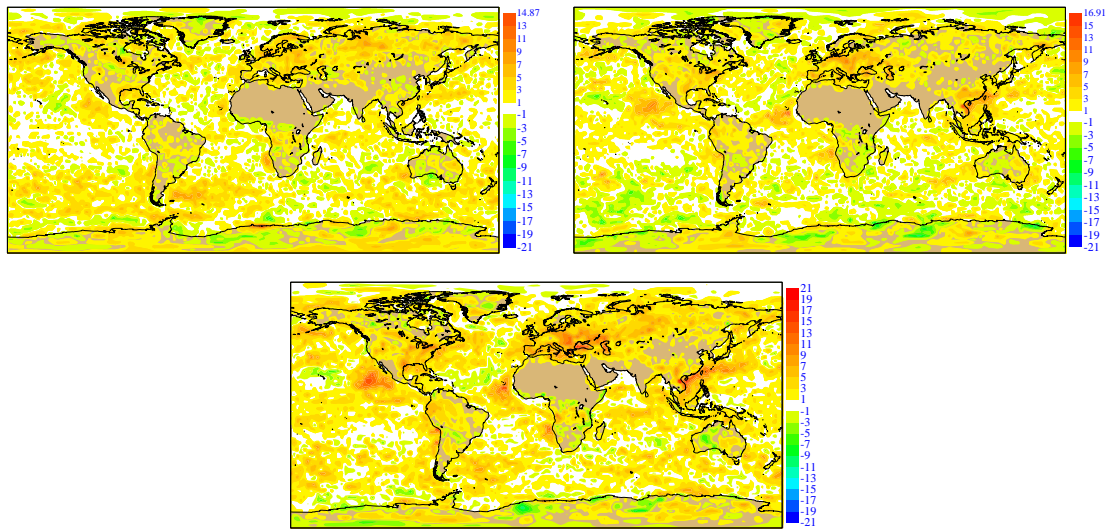
Figure 16: The monthly average over the last five days of 10-day forecasts of the differences AFDir-Ref (top left), AFInd-Ref (top right), AFDirInd-Ref (middle) for downward shortwave radiation at the surface (in Wm^{-2} for March 2011, for forecasts using the relevant analyzed aerosols in their initial conditions, but keeping them fixed afterwards.
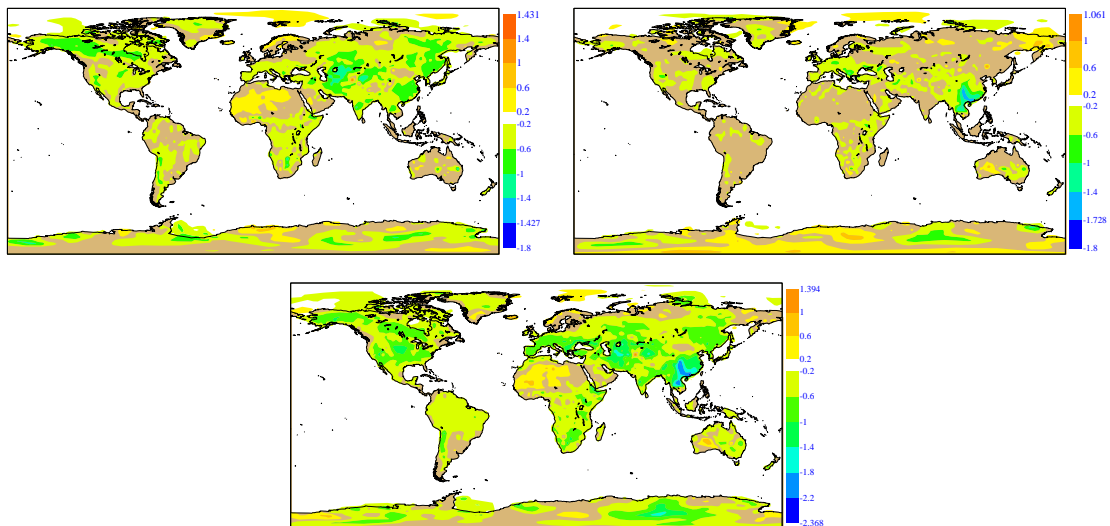
Figure 17: The monthly average over the last five days of 10-day forecasts of the differences AFDir-Ref (top left), AFInd-Ref (top right), AFDirInd-Ref (middle) for the surface skin temperature (in K) for March 2011, for forecasts using the relevant analyzed aerosols in their initial conditions, but keeping them fixed afterwards.
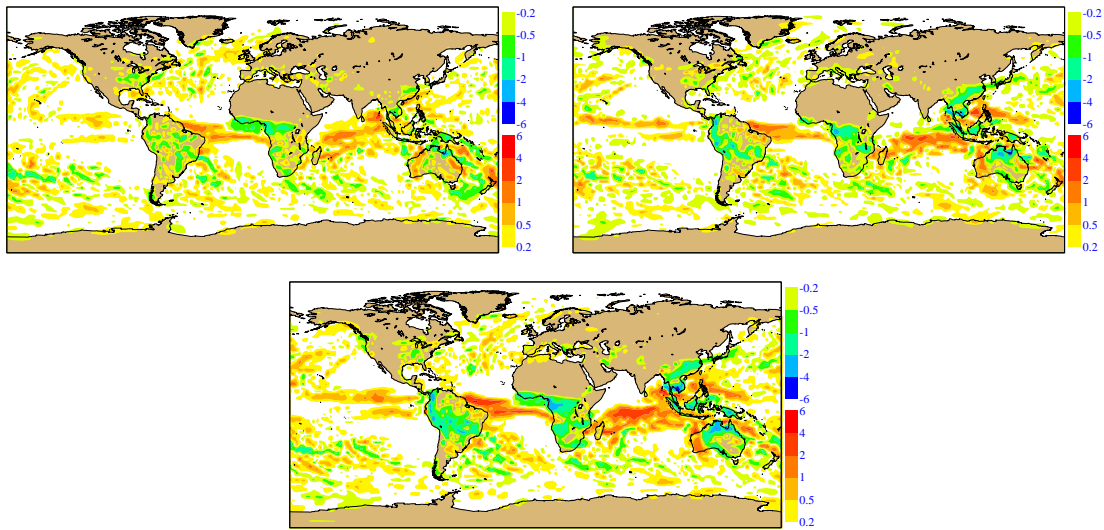
Figure 18: The monthly average over the last five days of 10-day forecasts of the differences AFDir-Ref (top left), AFInd-Ref (top right), AFDirInd-Ref (middle) for the total precipitation (in mmday^{-1}) for March 2011, for forecasts using the relevant analyzed aerosols in their initial conditions, but keeping them fixed afterwards.

the Northern hemisphere is shown. First, for all these objective scores for which the reference is the ECMWF operational analysis, the scores for a given configuration *Dir*, *Ind* or *DirInd* do not depend much whether the initial conditions are taken from the dedicated analysis (respectively, *FPDir*, *FPInd* or *FPDirInd*) or started from the *Ref* analysis (respectively, FP_RDir, FP_RInd or $FP_RDirInd$). Second, the scores obviously reflects the features already discussed in the previous sections, with the impact on surface temperature seen in 4.3.2 reflected in the results for mean error at 850 hPa.

4.5 Comparison with synoptic observations

The forecasts *Ref*, *FPDir*, *FPInd*, and *FPDirInd* have also been compared to the synoptic observations of 2-metre temperature, 2-metre dew point temperature, 10-metre wind, total cloudiness available over the synoptic network of meteorological observations. A comparison of the results of such comparisons for the 2-m temperature (*2mT*) and total cloudiness (*TCC*), for the *Ref* and the *FPDirInd* sets of forecasts is presented in Table 1 for three areas, Europe and two other (Africa, and South-East Asia) showing large aerosol signals in the figures discussed in the previous sections. Table 1 also presents the results for 12, 24, 60, 72, 108 and 120 hours into the forecasts allowing to see how the errors develop with forecast length and how they vary with the diurnal cycle. Looking first at the total cloudiness, the bias behaves differently over the three areas: for 00 UTC (corresponding to 12, 60 and 108 hours into the forecasts), the TCC bias steadily increases over Europe, increases then flattens over Africa, slowly increases over S.E. Asia, with similar behaviours for 12 UTC (24, 72, 120 hours into the forecasts). This pattern is seen for TCC for both *Ref* and *FPDirInd*. For *2mT*, a strong increasing cooling occurs over Europe with the forecast length, whether considering 00 UTC or 12 UTC hours). A similar cooling trend, but much weaker, also affects the African area. S.E. Asia, on the other hand, displays a warming trend both for 00 UTC (going from -0.42 to -0.29 to -0.18 K) and 12 UTC (going from -0.10 to 0.11 to 0.18 K) for *Ref*, but a small cooling trend for *FPDirInd* (going from -0.66 to -084 to -0.85 K at 00 UTC, and from -0.24 to -0.27 to -0.30 K at 12 UTC). Whereas these results show higher biases for *FPDirInd* relative to *Ref*, the standard deviation (*StDev*) and mean absolute error (*MAE*) results present a different pattern with

these two parameters indicating a better fit to observations for the forecasts with interactive prognostic aerosols.

EUROPE Lead Time	NObs TCC	Bias TCC	StDev TCC	MAE TCC	NObs 2mT	Bias 2mT	StDev 2mT	MAE 2mT
Ref +12	29493	-0.02	2.45	1.59	34339	0.20	2.01	1.51
DirInd +12		0.05	2.43	1.59		-0.05	1.96	1.46
Ref +24	22928	0.21	3.09	1.97	31335	-0.76	2.44	1.89
DirInd +24		0.36	3.04	1.95		-0.75	2.41	1.86
Ref +60	29444	0.08	2.91	1.96	34316	-0.01	2.41	1.83
DirInd +60		0.25	2.86	1.93		-0.46	2.32	1.81
Ref +72	22916	0.36	3.50	2.33	31344	-0.95	2.74	2.19
DirInd +72		0.57	3.45	2.31		-1.04	2.71	2.19
Ref+108	29486	0.23	3.19	2.22	34333	-0.27	2.71	2.09
DirInd+108		0.43	3.22	2.26		-0.81	2.65	2.14
Ref+120	22936	0.47	3.76	2.60	31361	-1.18	3.13	2.57
DirInd+120		0.72	3.78	2.65		-1.32	3.13	2.60

Table 1: Comparison of the Ref and FPDirInd sets of forecasts against synoptic station measurements of total cloudiness (TCC) and 2-metre temperature (2mT) over Europe. NObs refers to the number of observations available over the month of March 2011. +12, ..., +120 correspond to the different forecast lead times.

AFRICA Lead Time	NObs TCC	Bias TCC	StDev TCC	MAE TCC	NObs 2mT	Bias 2mT	StDev 2mT	MAE 2mT
Ref +12	12848	-0.59	2.63	1.92	13554	0.01	2.63	1.85
DirInd +12		-0.58	2.63	1.92		-0.15	2.61	1.84
Ref +24	9302	-0.07	3.12	2.14	11075	-0.93	2.42	2.01
DirInd +24		-0.04	3.12	2.13		-0.76	2.34	1.90
Ref +60	12795	-0.70	2.84	2.13	13509	-0.06	2.82	2.01
DirInd +60		-0.70	2.90	2.16		-0.34	2.81	2.06
Ref +72	9260	-0.13	3.36	2.34	11040	-1.02	2.58	2.15
DirInd +72		-0.21	3.38	2.36		-0.89	2.51	2.06
Ref+108	12761	-0.69	3.07	2.32	13470	-0.08	3.06	2.22
DirInd+108		-0.69	3.12	2.35		-0.38	3.04	2.28
Ref+120	9232	-0.04	3.51	2.50	11011	-1.08	2.76	2.31
DirInd+120		-0.17	3.56	2.55		-0.99	2.71	2.25

Table 1 (continued): Comparison of the Ref and FPDirInd sets of forecasts against synoptic station measurements of total cloudiness (TCC) and 2-metre temperature (2mT) over Africa. NObs refers to the number of observations available over the month of March 2011. +12, ..., +120 correspond to the different forecast lead times.

S.E.ASIA Lead Time	NObs TCC	Bias TCC	StDev TCC	MAE TCC	NObs 2mT	Bias 2mT	StDev 2mT	MAE 2mT
Ref +12	21143	0.08	2.62	1.62	22663	-0.42	2.53	1.88
DirInd +12		0.15	2.58	1.58		-0.66	2.47	1.88
Ref +24	20944	-0.03	2.67	1.65	22613	-0.10	2.62	1.89
DirInd +24		0.06	2.62	1.60		-0.24	2.58	1.86
Ref +60	21150	0.09	2.81	1.76	22669	-0.29	2.85	2.10
DirInd +60		0.20	2.79	1.75		-0.84	2.75	2.15
Ref +72	20987	0.04	2.88	1.80	22652	0.11	2.87	2.10
DirInd +72		0.11	2.87	1.79		-0.27	2.80	2.05
Ref+108	21151	0.12	3.07	1.97	22667	-0.18	3.04	2.24
DirInd+108		0.20	3.03	1.94		-0.85	2.93	2.31
Ref+120	21013	0.08	3.08	1.96	22668	0.18	3.30	2.22
DirInd+120		0.11	3.05	1.94		-0.30	2.95	2.18

Table 1 (continued): Comparison of the Ref and FPDirInd sets of forecasts against synoptic station measurements of total cloudiness (TCC) and 2-metre temperature (2mT) over South-East Asia. NObs refers to the number of observations available over the month of March 2011. +12, ..., +120 correspond to the different forecast lead times.

5 Impact of direct and indirect aerosol effects in 10-day forecasts with analyzed but fixed aerosols

In section 4, the forecasts were obtained using fully prognostic aerosols. In view of the rather limited impact on standard meteorological scores (very little impact on anomaly correlation of geopotential, limited impact on r.m.s.e. and mean error of temperature, no impact on wind scores), one can wonder whether introducing prognostic aerosols in a NWP system is really worthwhile. In particular, adding 12 prognostic variables to the five three-dimensional variables (temperature, humidity, vorticity and divergence, ozone) and the prognostic surface pressure, operationally carried out in the ECMWF IFS increases significantly (a factor between two and three depending on the exact configuration) both the required memory by the model, and the computer time required to get a forecast.

Consideration has therefore been given to an alternate solution aiming in particular at saving computer time. This includes using the relevant analyzed aerosol distributions (*Dir*, *Ind*, *DirInd*) and keep them fixed during the 10-day length of the forecasts. Using this approach allows to have the initial conditions close to the observations, and if meteorological patterns were dependent on the aerosol distributions (still a rather debatable assumption), to have a first-order representation of the aerosol "forcing" for the potential interactions with radiation and cloud processes.

Whereas this configuration (hereafter referred to as *AF*) requires more memory (to account for the additional 11 analyzed aerosol variables), the impact on the run time is much smaller than having fully prognostic aerosols, as these aerosols are not transported by either the dynamics or the vertical advective or convective processes. However, depending on the configuration, they can interact with radiation (*AFDir*) and/or cloud processes (*AFInd* or *AFDirInd*).

Figures 13 to 18 present for these forecasts the total cloudiness (Fig. 13), low-level (Fig. 14) and high-level cloudiness (Fig.15), downward shortwave radiation at the surface (Fig.16), surface skin temperature (Fig.17) and total precipitation (Fig.18). In each of these figures, the differences *AFDir-Ref*, *AFInd-*

Ref, *AFDirInd-Ref* are presented for forecasts with the aerosols varying from day-to-day according to their analyses but fixed at their analyzed distributions during the subsequent 10-day forecasts.

Not surprisingly, a number of patterns seen in Figures 13 to 18 are reminiscent of what was shown in Figures 6 to 11. In Figures 13 and 15, the decrease in cloudiness over equatorial Africa for *AFDir* and *AFDirInd* is similar in magnitude to what was seen in Figures 6 and 8. However, there are differences with the *Ind-Ref* signal over the tropical oceans being reversed from a decrease in Figures 6 and 8 to an increase in Figures 13 and 15. The decrease in low-level cloudiness over the oceans seen in *Ind-Ref* in Figure 7 becomes a increase in Figure 14. There is also a much increased contrast in the various geographical signals. Overall, the pattern of decrease and increase in *DirInd-Ref* is maintained, but with somewhat larger amplitudes, for analyzed then fixed aerosols.

For skin temperature, comparing Figures 17 and 10 shows stronger contrast with the analyzed then fixed aerosols that with the fully prognostic ones. The cooling seen for *Dir-ref* over most of the Northern hemisphere is more pronounced, and is further emphasized when considering *DirInd-Ref*. The overall warming over the Sahara and the Arabian peninsula is reduced.

Similar results can be found for total precipitation, comparing Figures 18 and 11. The large-scale geographical patterns are similar, but overall the amplitude of the signals is emphasized with analyzed then fixed aerosols. The decrease in precipitation over equatorial Africa is present as in the increase over the Indian ocean. A further decrease in seen over South America and parts of Australia.

However, although there is a reasonable consistency in the results seen for cloudiness, skin temperature and precipitation, between results obtained with fully prognostic aerosols and those with analyzed then fixed aerosols, a different result is obtained for downward shortwave radiation at the surface, comparing Figures 9 and 16.

As for the FP and FP_R forecasts, the standard objective scores for anomaly correlation of the geopotential at 1000 and 500 hPa, root mean square and mean error of temperature and wind at 850, 500, 200 hPa were produced for the Northern and Southern hemispheres (20°-pole), the tropical area (20^oN-20^oS), and various areas (Europe, North America, South America, Africa, North Asia, South-East Asia). Only scores for temperature at 850 hPa are shown in Figure 19, and can therefore be compared to those in Figure 12. For the Northern and Southern hemispheres where anomalies are more likely to be driven by the dynamics than by the physics, the behaviour of the r.m.s. errors are very similar in both the FP-FP_R and *AF* configurations. In the tropics, where the details of temperature field is much more influenced by the physics, the spread in r.m.s.e. between the *Ref*, *Dir Ind* and *DirInd* configurations is bigger in the *AF* configuration (Fig.19) than int the FP-FP_R configurations (Fig.12), potentially indicating a mismatch between the aerosols and cloud forcing. THis also shows in mean error temperature scores: Scores with the *AF* configurations are generally worse than those with the FP or FP_R configuration, with the errors at day 10 bigger with the *AF* than with the FP-FP_R configurations, when compared to the operational analysis.

6   Discussion, concluding remarks and perspectives

Over the last two decades, numerous developments in modelling aerosol processes and their links to cloud and radiative processes have made the aerosols major actors in general circulation models used for climate simulations and projections (AMIP, IPCC AR5, REF), but also in studies of the interactions of aerosols with clouds carried on with large-eddy simulations and cloud resolving models (REF). More recently, aerosols have appeared as prognostic variables in numerical weather prediction (NWP) analysis
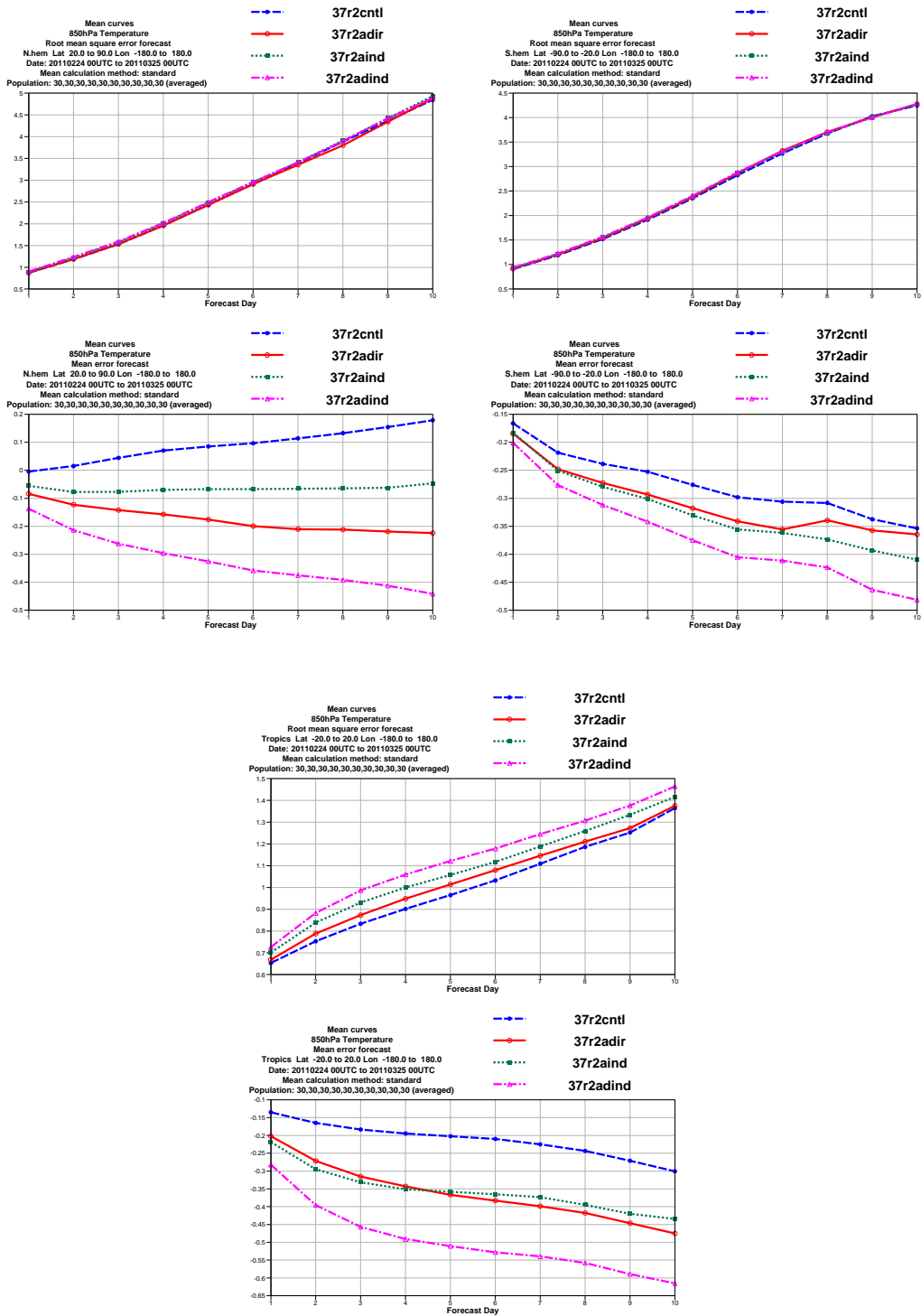
Figure 19: The root mean square error and the mean error of the temperature at 850 hPa for the forecasts for March 2011, for the Northern (two plots on the left), the Southern hemisphere (top plots on the right), and the tropical area (two plots lower down in the middle). For each set of plots, the r.m.s. error plot is on top and the mean error plot is at the bottom. Curves correspond to Ref (blue), AFDir (red), AFInd (green), and AFDirInd (purple). Dir, Ind and DirInd here refer to the interactions with radiation and/or cloud processes but with the aerosols fixed during the 10-day forecasts from the relevant analyses.

and forecast systems (e.g., Zhang et al., 2008, Benedetti et al., 2009, Morcrette et al., 2009)

How much detail of aerosol processes is actually required to carry out a proper weather forecast remains an important question, given the time constraints of an operational system providing day-to-day analyses of the global atmosphere and subsequent forecasts. At ECMWF, an increase in the level of details in the description of the interactions between aerosols, clouds, radiation and precipitation corresponds to an increase in the number of prognostic variables to be dealt with, which typically contributes to at least a factor of two increase in the time taken by a given forecast, for a 12-aerosol-related variable system such as MACC. Given this constraint, such a system can therefore only be run at a lower horizontal (and possibly vertical) resolution than the headline system (currently run over 10-days at T_L1279 L91 resolution (a grid of roughly 15x15 km^2 and 91 vertical levels spanning from the surface to 0.01 hPa).

The present study was an attempt using the MACC/ECMWF IFS to address this question. For the period 24 February to 31 March 2011, analysis and subsequent forecasts were carried out with various representations of the interactions between aerosols, radiation, clouds and precipitation.

First, it was shown that the distribution of the various prognostic aerosols can be rather different from the climatology of aerosols currently used in the operational ECMWF IFS.

Second, given the configuration of the MACC/ECMWF aerosol system, having the full interactions between aerosols and radiation and/or clouds to run the analysis appear not to bring marked improvements on the subsequent forecasts compared to an aerosol analysis where the prognostic aerosols do not interact with radiation and/or cloud processes. The differences in the forecasts are linked to the differences in the treatment of the interactions in the forecast model.

Third, when interactions with radiation (*Dir*) and/or liquid water clouds (*Ind*, *DirInd*) are considered, the first order response in the *DirInd* forecasts is roughly the sum of the direct and indirect effects.

Fourth, given the length of the experimentation reported in this study (a period covering a month of analysis and subsequent forecasts), the impact on traditional meteorological scores is almost negligible on geopotential, and only noticeable in r.m.s. errors of temperature at lower tropospheric levels (850 hPa) in the 20^oN-20^oS tropical band and mean errors of temperature at similar lower tropospheric levels in the Northern and Southern hemispheres and in the tropical band.

Fifth, when compared to synoptic observations, the fit of total cloudiness to observations is slightly degraded in terms of bias, for the three areas (Europe, Africa, South-East Asia). In terms of standard deviation and mean absolute error of total cloudiness, *FPDirInd* somewhat deteriorates the scores for Africa and Europe, but clearly improves them for South-East Asia. Similar results are seen for two-metre temperature, with a degradation in terms of bias to observations but a general improvement over the three areas in terms of standard deviation and mean absolute errors,

Sixth, compared to 10-day forecasts with fully interactive aerosols, 10-day forecasts using analyzed aerosols in the initial conditions, kept fixed during the forecasts, display more constrasting responses for most of the fields analyzed (surface temperature, precipitation, total, low- and high-level cloudiness) and worse r.m.s. errors in temperature at 850 hPa.

This last conclusion particularly relates to the role of the fire-related aerosols in the variability of the aerosol optical depth. Analyzed then fixed aerosols tend to create strong centres of aerosol-related radiative and cloud anomalies whose persistence over the length of the forecasts might have negative impact on the forecast quality. With fully prognostic aerosols, the fire-related aerosols might still be not optimally defined, but the interactions between aerosols, radiation and cloud processes are likely to mitigate their overall effects, whereas aerosols fixed at their analyzed values create a much stronger permanent

forcing.

In conclusion, fully prognostic aerosols in both the analyses and the subsequent forecasts appear the most attractive solution to capture the details of the interactions, but the cost in both computer memory and execution time makes their operational adoption a scientific challenge, as trade-off between introducing fully prognostic aerosols in the NWP system and/or for example further increase in the horizontal and/or vertical resolution for the presently operational high-resolution T_L1279 L91 and Ensemble Prediction System at T_L639 L62 will have to be decided upon.

7   Acknowledgements

References

http://dataipsl.ipsl.jussieu.fr/AEROCOM/

http://gems.ecmwf.int/d/products/aer/verif/

http://gems.ecmwf.int/d/products/aer/realtime/

http://www.gmes-atmosphere.eu/d/services/gac/nrt/

Ackerman, T.P. and O.B. Toon, 1981: Absorption of visible radiation in atmosphere containing mixtures of absorbing and non-absorbing particles. *Appl. Opt.*, **20**, 3661-367.

Benedetti, A., J.-J. Morcrette, O. Boucher, A. Dethof, R.J. Engelen, M. Fisher, H. Flentjes, N. Huneeus, L. Jones, J.W. Kaiser, S. Kinne, A. Mangold, M. Razinger, A.J. Simmons, M. Suttie, and the GEMS-AER team, 2009: Aerosol analysis and forecast in the ECMWF Integrated Forecast System: Data assimilation. *J. Geophys. Res.*, **114**, D13205, doi:10.1020/2008JD011115.

Boucher, O., M. Pham, and C. Venkataraman, 2002: *Simulation of the atmospheric sulfur cycle in the LMD GCM. Model description, model evaluation, and global and European budgets.* IPSL, Note 23, 26 pp. (available at http://www.ipsl.jussieu.fr/ poles/ Modelisation/ NotesSciences.htm.)

Chin, M., D.J. Jacob, G.M. Gardner, and P.A. Spiro, 1996: A global three-dimensional model of tropospheric sulfate. *J. Geophys. Res.*, **101**, 18667-18690.

Chin, M., P. Ginoux, S. Kinne, O. Torres, B.N. Holben, B.N. Duncan, R.V. Martin, J.A. Logan, A. Higurashi, and T. Nakajima, 2002: Tropospheric aerosol optical thickness from the GOCART model and comparisons with satellite and Sun photometer measurements. *J. Atmos. Sci.*, **59**, 461-483.

Clarke, A. D., W. G. Collins, P. J. Rasch, V. N. Kapustin, K. Moore, S. Howell, H. E. Fuelberg, 2001: Dust and pollution transport on global scales: Aerosol measurements and model predictions. *J. Geophys. Res.*, **106D**, 32555-32570, doi: 10.1029 /2000JD900842.

Collins, W. D., P. J. Rasch, B. E. Eaton, B. V. Khattatov, J.-F. Lamarque, C. S. Zender, 2001: Simulating aerosols using a chemical transport model with assimilation of satellite aerosol retrievals: Methodology for INDOEX, *J. Geophys. Res.*, **106D**, 7313-7336, doi: 10.1029 /2000JD900507.

Dee, D., and S. Uppala, 2008: Variational bias correction in ERA-Interim. *ECMWF Technical Memorandum*, **575**, 26 pp.

Dentener, F. J. Feichter, and A. Jeuken, 1999: Simulation of the transport of 222Rn using on-line and off-line models at different horizontal resolutions: A detailed comparison with observations. *Tellus*, **51B**, 573-602.

Dentener, F., S. Kinne, T. Bond, O. Boucher, J. Cofala, S. Generoso, P. Ginoux, S. Gong, J. J. Hoelzemann, A. Ito, L. Marelli, J. E. Penner, J.-P. Putaud, C. Textor, M. Schulz, G. R. van der Werf, and J. Wilson, 2006: Emissions of primary aerosol and precursor gases in the years 2000 and 1750 prescribed data-sets for AeroCom. *Atmos. Chem. Phys.*, **6**, 4321-4344.

Dubovik, O., B. Holben, T.F. Eck, A. Smirnov, Y.J. Kaufman, M.D. King, D. Tanré, and I. Slutsker, 2002: Variability of absorption and optical properties of key aerosol types observed in worldwide locations *J. Atmos. Sci.*, **59**, 590-608.

Feichter, J., and U. Lohmann, 1999: Can relaxation technique be used to validate clouds and sulphur species in a GCM? *Quart. J. Roy. Meteor. Soc.*, **125**, 1277-1294.

Genthon, C., 1992: Simulations of desert dust and sea salt aerosols in Antarctica with a general circulation model of the atmosphere. *Tellus*, **44B**, 371-389.

Gong, S.L., L.A. Barrie, and J.-P. Blanchet, 1997: Modeling sea-salt aerosols in the atmosphere. 1. Model development. *J. Geophys. Res.*, **102D**, 3805-3818.

Gong, S.L., L.A. Barrie, J.-P. Blanchet, K.v. Salzen, U. Lohmann, G. Lesins, L. Spacek, L.M. Zhang, E. Girard, H. Lin, R. Leaitch, H. Leighton, P. Chylek, and P. Huang, 2003: Canadian Aerosol Module: A Size Segregated Simulation of Atmospheric Aerosol Processes for Climate and Air Quality Models 1. Module Development, *J. Geophys. Res.*, **108D**, 4007, doi: 10.1029 /2001JD002002.

Grini, A., G. Myrhe, J.K. Sundet, and I.S.A. Isaksen, 2002: Modeling the annual cycle of sea salt in the global 3D model Oslo CTM2: Concentrations, fluxes and radiative impact. *J. Climate*, **15**, 1717-1730.

Guelle, W., Y.J. Balkanski, M. Schulz, F. Dulac, and P. Monfray, 1998: Wet deposition in a global size-dependent aerosol transport model. 1. Comparison of a 1 year 210Pb simulation with ground measurements. *J. Geophys. Res.*, **103D**, 11,429-11,445.

Guelle, W., Y.J. Balkanski, J. Dibb, M. Schulz, and F. Dulac, 1998: Wet deposition in a global size-dependent aerosol transport model. 2. Influence of the scavenging scheme on ^{210}Pb vertical profiles, surface concentrations and deposition. *J. Geophys. Res.*, **103D**, 28875-28891.

Guelle, W., Y.J. Balkanski, M. Schulz, B. Marticorena, G. Bergametti, C. Moulin, R. Arimoto, and K.D. Perry, 2000: Modeling the atmospheric distribution of mineral aerosol: Comparison with ground and satellite observations for yearly and synoptic timescales over the North Atlantic. *J. Geophys. Res.*, **105D**, 1997-2012.

Hess, P. Koepke, and I. Schult, 1998: Optical properties of aerosols and clouds: The software package OPAC. *Bull. Amer. Meteor. Soc.*, **79**, 831-844.

Hollingsworth, A., R.J. Engelen, C. Textor, A. Benedetti, O. Boucher, F. Chevallier, A. Dethof, H. Elbern, H. Eskes, J. Flemming, C. Granier, J.W. Kaiser, J.-J. Morcrette, P. Rayner, V.-H. Peuch, L. Rouil, M. Schultz, A. Simmons, and the GEMS Consortium, 2008: The Global Earth-system Monitoring using Satellite and in-situ data (GEMS) project: Towards a monitoring and forecasting system for atmospheric composition. *Bull. Amer. Meteor. Soc.*, **89**, 1147-1164, doi: 10.1175 /2008BAMS2355.1

Huneeus, N., and O. Boucher, 2007: One-dimensional variational retrieval of aerosol extinction coefficient from synthetic LIDAR and radiometric measurements. *J. Geophys. Res.*, **112**, D14303, doi: 10.1029 /2006/JD007625.

Iacono, M. J., J. S. Delamere, E. J. Mlawer, S. A. Clough, J.-J. Morcrette, and Y.-T. Hou, 2004: Development and evaluation of RRTMG$_{SW}$, a shortwave radiative transfer model for general circulation model applications. *Proceedings of the 14th Atmospheric Radiation Measurement (ARM) Science Team Meeting*, Albuquerque, New Mexico, March 22-26, 2004.

Jeuken, A.B.M., P.C. Siegmund, L.C. Heijboer, J. Feichter, and L. Bengtsson, 1996: On the potential of assimilating meteorological analyses in a global climate model for the purpose of model validation. *J. Geophys. Res.*, **101**, 16939-16950.

Joussaume, S., 1990: Three-dimensional simulations of the atmospheric cycle of desert dust particles using a general circulation model. *J. Geophys. Res.*, **95D**, 1909-1941.

Kaiser, J.W., M. Suttie, J. Flemming, J.-J. Morcrette, O. Boucher, and M.G. Schultz, 2009: GLobal real-time fire emission estimates based on space-borne fire radiative power observations. *AIP Conf. Proc.*, **1100**, 645-648.

Kaiser, J. W., A. Heil, M.O. Andreae, A. Benedetti, N. Chubarova, L. Jones, J.-J. Morcrette, M. Razinger, M.G. Schultz, M. Suttie, and G.R. van der Werf, 2011: Biomass burning emissions estimated with a global fire assimilation system based on observed fire radiative power. *Biogeosciences Discuss.*, **8(4)**, 7339-7398.

Kinne S., U. Lohmann, J. Feichter, M. Schulz, C. Timmreck, S. Ghan, R. Easter, M. Chin, P. Ginoux, T. Takemura, I. Tegen, D. Koch, M. Herzog, J. Penner, G. Pitari. B. Holben, T. Eck, A. Smirnow, O. Dubovik, I. Slutsker, D. Tanré, O. Torres, M. Mishchenko, I. Geogdzhayev, D.A. Chu, and Y. Kaufman, 2003: Monthly averages of aerosol properties: A global comparison among models, satellite data, and AERONET ground data, *J. Geophys. Res.*, **108** (D20), 4634, doi:10.1029/2001JD001253.

Kinne, S., M. Schulz, C. Textor, S. Guibert, Y. Balkanski, S. E. Bauer, T. Berntsen, T. F. Berglen, O. Boucher, M. Chin, W. Collins, F. Dentener, T. Diehl, R. Easter, J. Feichter, D. Fillmore, S. Ghan, P. Ginoux, S. Gong, A. Grini, J. Hendricks, M. Herzog, L. Horowitz, I. Isaksen, T. Iversen, A. Kirkevåg, S. Kloster, D. Koch, J. E. Kristjansson, M. Krol, A. Lauer, J. F. Lamarque, G. Lesins, X. Liu, U. Lohmann, V. Montanaro, G. Myhre, J. Penner, G. Pitari, S. Reddy, Ø. Seland, P. Stier, T. Takemura, and X. Tie, 2006: An AeroCom initial assessment: Optical properties in aerosol component modules of global models. *Atmos. Chem. Phys.*, **6**, 1815-1834.

Lacis, A.A., 2001: Database of Aerosol Spectral Refractive Indices. $http://gacp.giss.nasa.gov/data_sets/$

Lee, S.S., and J.E. Penner, 2010: Aerosol effects on ice clouds: Can the traditional concept of aerosol indirect effects be applied to aerosol-cloud interactions in cirrus clouds? *Atmos. Chem. Phys.*, **10**, 10345-10358, doi: 10.5194/acp-10-10345-2010.

Li, Z., F. Niu, J. Fan, Y. Liu, D. Rosenfeld, and Y. Dang, 2011: Long-term impacts of aerosols on the vertical development of clouds and precipitation. *Nature Geophys.*, doi:10.1038/ngeo1313, 7 pp.

Liousse, C., J.E. Penner, C. Chuang, J.J. Walton, H. Eddleman, and H. Cachier, 1996: A global three-dimensional model study of carbonaceous aerosols. *J. Geophys. Res.*, **101**, 19,411-19,432.

Liu, M., D. L. Westphal, S. Wang, A. Shimizu, N. Sugimoto, J. Zhou, and Y. Chen, 2003: A high-resolution numerical study of the Asian dust storms of April 2001. *J. Geophys Res.*, **108D**, 8653, doi: 10.1029 /2002JD003178.

Lohmann, U. and. J. Feichter, 2001: Can the direct and and semi-direct compete with the indirect aerosol effect on a global scale? *Geophys. Res. Lett.*, **28**, 159-161.

Lohmann, U., 2002: Possible aerosol effects on ice clouds via contact nucleation. *J. Atmos. Sci.*, **59**, 647-656.

Lohmann, U., and B. Kärcher, 2002: First interactive simulations of cirrus clouds formed by homogeneous freezing in the ECHAM general circulation model. *J. Geophys. Res.*, **107B**, doi: 10.1029 /2001JD000767.

Lohmann U., and J. Feichter J., 2005: Global indirect aerosol effects: A review, *Atmos. Chem. Phys.*, **5**, 715-737.

Martin, G.M., D.W. Johnson, and A. Spice, 1994: The measurement and parameterization of effective radius of droplets in warm stratocumulus. textitJ. Atmos. Sci., **51**, 1823-1842.

Menon, S., A.D. Del Genio, D. Koch, and G. Tselioudis, 2002: GCM simulations of the aerosol indirect effect: Sensitivity to cloud parameterization and aerosol burden. *J. Atmos. Sci.*, **59**, 692-713.

Mlawer, E.J., S.J. Taubman, P.D. Brown, M.J. Iacono, and S.A. Clough, 1997: Radiative transfer for inhomogeneous atmospheres: RRTM, a validated correlated-k model for the longwave. *J. Geophys. Res.*, **102D**, 16,663-16,682.

Morcrette, J.-J., H.W. Barker, J.N.S. Cole, M.J. Iacono, and R. Pincus, 2008: Impact of a new radiation package, McRad, in the ECMWF Integrated Forecasting System. *Mon. Wea. Rev.*, **136**, 4773-4798, doi: 10.1175 /2008MWR2363.1

Morcrette, J.-J., O. Boucher, L. Jones, D. Salmond, P. Bechtold, A. Beljaars, A. Benedetti, A. Bonet, J.W. Kaiser, M. Razinger, M. Schulz, S. Serrar, A.J. Simmons, M. Sofiev, M. Suttie, A.M. Tompkins, A. Untch, 2009: Aerosol analysis and forecast in the ECMWF Integrated Forecast System: Forward modelling. *J. Geophys. Res.*, **114**, doi: 10.1029 /2008JD011235.

Morcrette, J.-J., A. Benedetti, L. Jones, J.W. Kaiser, M. Razinger, M. Suttie, 2011: Prognostic aerosols in the ECMWF IFSL MACC vs. GEMS aerosols. manuscript, 32 pp., December 2011.

Penner, J.E., S.Y. Zhang, M. Chin, C.C. Chuang, J. Feichter, Y. Feng, I.V. Geogdzhayev, P. Ginoux, M. Herzog, A. Higurashi, D. Koch, C. Land, U. Lohmann, M. Mishchenko, T. Nakajima, G. Pitari, B. Soden, I. Tegen, and L. Stowe, 2002: A comparison of model- and satellite-derived aerosol optical depth and reflectivity. *J. Atmos. Sci.*, **59**, 441-460.

Rasch, P. J., W. D. Collins, B. E. Eaton, 2001: Understanding the Indian Ocean Experiment (INDOEX) aerosol distributions with an aerosol assimilation, *J. Geophys. Res.*, **106D**, 7337-7356, doi: 10.1029 /2000JD900508.

Reddy, M.S., O. Boucher, C. Venkataraman, S. Verma, J.-F. Léon, N. Bellouin, and M. Pham, 2004: General circulation model estimates of aerosol transport and radiative forcing during the Indian Ocean Experiment. *J. Geophys. Res.*, **109**, D16205, doi: 10.1029 /2004JD004557.

Reddy M. S., O. Boucher, N. Bellouin, M. Schulz, Y. Balkanski, J.-L. Dufresne, M. Pham, 2005: Estimates of global multicomponent aerosol optical depth and direct radiative perturbation in the Laboratoire de Meteorologie Dynamique general circulation model, *J. Geophys. Res.*, **110D**, S16, doi: 10.1029 /2004JD004757.

Rodwell, M.J., and T. Jung, 2008: Understanding the local and global impacts of model physics changes: An aerosol example. *Quart. J. Roy. Meteor. Soc.*, **134**, 1479-1497, doi: 10.1002/qj.298

Rotstayn, L.D., and J.E. Penner, 2001: Indirect aerosol forcing, quasi forcing, and climate response. *J. Climate*, **14**, 2960-2975.

Schulz, M., C. Textor, S. Kinne, Y. Balkanski, S. Bauer, T. Berntsen, T. Berglen, O. Boucher, F. Dentener, S. Guibert, I. S. A. Isaksen, T. Iversen, D. Koch, A. Kirkevåg, X. Liu, V. Montanaro, G. Myhre, J. E. Penner, G. Pitari, S. Reddy, Ø. Seland, P. Stier, and T. Takemura, 2006: Radiative forcing by aerosols as derived from the AeroCom present-day and pre-industrial simulations. *Atmos. Chem. Phys.*, **6**, 5225-5246.

Sekiyama, T.T., T.Y. Tanaka, A. Shimizu, and T. Miyoshi, 2009: Data assimilation of CALIPSO aerosol observations. *Atmos. Chem. Phys. Discuss.*, **9**, 5785-5808.

Shao, Y., Y. Yang, J. Wang, Z. Song, L.M. Leslie, C. Dong, Z. Zhang, Z. Lin, Y. Kanai, S. Yabuki, and Y. Chun, 2003: Northeast Asian dust storms: Real-time numerical prediction and validation. *J. Geophys. Res.*, **108**, 4691, doi: 10.1029 /2003JD003667.

Simmons, A.J., 2010: Monitoring Atmospheric Composition and Climate, *ECMWF Newsletter*, **123**, 10-13.

Spichtinger, P., and K.M. Gierens, 2009: Modelling of cirrus clouds. Part 2: Competition of different nucleation mechanisms. *Atmos, CHem. Phys.*, **9**, 2319-2334, doi: 10.5194/acp-9-2319-2009.

Sundqvist, H., 1988: Parameterization of condensation and associated clouds in models for weather prediction and general circulation simulation. textitPhysically Based Modelling and Simulation of Climate and Climate Change, M.E. Schlesinger, Ed., Kluwer, 433-461.

Sundqvist, H., E. Berge, and J.E. Kristjánsson, 1989: Condensation and cloud parameterization studies with a mesoscale numerical prediction model. *Mon. Wea. Rev.*, **117**, 1641-1657.

Tang, I. N., 1997: Thermodynamic and optical properties of mixed-salt aerosols of atmospheric importance, *J. Geophys. Res.*, **102D**, 1883-1894, doi: 10.1029 /96JD03085.

Tang, I.N., and H.R. Munkelwitz, 1994: Water activities, densities and refractive indices of aqueous sulfates and sodium nitrate droplets of atmospheric importance. *J. Geophys. Res.*, **99**, 18,801-18,808.

Tanré, D., J.-F. Geleyn, and J.M. Slingo, 1984: First results of the introduction of an advanced aerosol-radiation interaction in the ECMWF low resolution global model, in *Aerosols and their Climatic Effects*, H.E. Gerber and A. Deepak, eds., A. Deepak Publishing, Hampton, Va, USA, 133-177.

Tegen, I., and I. Fung, 1994: Modeling of mineral dust in the atmosphere: Sources , transport, and optical thickness. *J. Geophys. Res.*, **99**, 22897-22914.

Tegen, I, P. Hoorig, M. Chin, I. Fung, D. Jacob, and J. Penner, 1997: Contribution of different aerosol species to the global aerosol extinction optical thickness: Estimates from model results. *J. Geophys. Res.*, **102**, 23,895-23,915.

Textor, C., M. Schulz, S. Guibert, S. Kinne, Y. Balkanski, S. Bauer, T. Berntsen, T. Berglen, O. Boucher, M. Chin, F. Dentener, T. Diehl, J. Feichter, D. Fillmore, P. Ginoux, S. Gong, A. Grini, J. Hendricks, L. Horowitz, P. Huang, I. S. A. Isaksen, T. Iversen, S. Kloster, D. Koch, A. Kirkevåg, J. E. Kristjansson, M. Krol, A. Lauer, J. F. Lamarque, X. Liu, V. Montanaro, G. Myhre, J. E. Penner, G. Pitari, M. S. Reddy, Ø. Seland, P. Stier, T. Takemura, and X. Tie, 2007: The effect of harmonized emissions on aerosol properties in global models: an AeroCom experiment. *Atmos. Chem. Phys.*, **7**, 4489-4501.

Textor, C., M. Schulz, S. Guibert, S. Kinne, Y. Balkanski, S. Bauer, T. Berntsen, T. Berglen, O. Boucher, M. Chin, F. Dentener, T. Diehl, R. Easter, H. Feichter, D. Fillmore, S. Ghan, P. Ginoux, S. Gong, A.

Grini, J. Hendricks, L. Horowitz, P. Huang, I. Isaksen, I. Iversen, S. Kloster, D. Koch, A. Kirkevåg, J. E. Kristjansson, M. Krol, A. Lauer, J. F. Lamarque, X. Liu, V. Montanaro, G. Myhre, J. Penner, G. Pitari, S. Reddy, Ø. Seland, P. Stier, T. Takemura, and X. Tie, 2006: Analysis and quantification of the diversities of aerosol life cycles within AeroCom. *Atmos. Chem. Phys.*, **6**, 1777-1813.

Tompkins, A.M., 2005: *A revised cloud scheme to reduce the sensitivity to vertical resolution*. ECMWF Research Dept Technical Memorandum, 20 pp.

Tompkins, A.M., C. Cardinali, J.-J. Morcrette, and M. Rodwell, 2005: Influence of aerosol climatology on forecasts of the African Easterly Jet. *Geophys. Res. Letters*, **32**, L10801, doi: 10.1029 /2004GL022189.

Twomey, W., 1974: Pollution and the planetary albedo. *Atmos. Environ.*, **8**, 1251-1256.

Zhang, J., J.S. Reid, and B.N. Holben, 2005: An analysis of potential cloud artifacts in MODIS over ocean aerosol optical thickness products. *Geophys. Res. Lett.*, **32**, L15803, doi: 10.1029 /2005GL023254.

Zhang, J. and J.S. Reid., 2006: MODIS Aerosol Product Analysis for Data Assimilation: Assessment of Level 2 Aerosol Optical Thickness Retrievals. *J. Geophys. Res.*, **111**, D22207, doi: 10.1029 /2005JD006898.

Zhang, J., J.S. Reid, D. Westphal, N. Baker, and E. Hyer, 2008: A System for Operational Aerosol Optical Depth Data Assimilation over Global Oceans. *J. Geophys. Res.*, **113**, D10208, doi: 10.1029 /2007JD009065.

Zhao, T. L., S. L. Gong, X. Y. Zhang, and I. G. Mckendry, 2003: Modeled size segregated wet and dry deposition budgets of soil dust aerosol during ACE-Asia 2001: Implications for trans-Pacific transport. *J. Geophys Res.*, **108**, 8665, doi: 10.1029 /2002JD003363.

Zhou, C.H., S.L. Gong, X.Y. Zhang, Y.Q. Wang, T. Niu, H.L. Liu, T.L. Zhao, Y.Q. Yang, and Q. Hou, 2008: Development and evaluation of an operational SDS forecasting system for East Asia: CUACE/Dust. *Atmos. Chem. Phys.*, **8**, 787-798.